

SCUOLA DI SCIENZE
Dipartimento di Chimica Industriale "Toso Montanari"

Corso di Laurea Magistrale in

Chimica Industriale

Classe LM-71 - Scienze e Tecnologie della Chimica Industriale

A systematic study on Paclitaxel
prodrugs synthesis: novel tools for bio-
responsive nanoparticles preparation

Tesi di laurea sperimentale

CANDIDATO

Martina Mamone

RELATORE

Prof.ssa Mariafrancesca Fochi

CORRELATORE

Dott.ssa Claudia Ferroni

ABSTRACT

Il cancro è una patologia estremamente complessa ed eterogenea, e, nonostante la ricerca di nuove strategie terapeutiche antitumorali abbia compiuto notevoli progressi, rimane la seconda causa di morte a livello globale. Ogni neoplasia richiede un approccio differente e personalizzato, ed i trattamenti convenzionali (rimozione chirurgica, radioterapia, chemioterapia o terapia ormonale) presentano numerose limitazioni, fra cui scarsa selettività con conseguente tossicità sistemica, immunodepressione e insorgenza di fenomeni di resistenza. Al fine di superare tali limiti, la ricerca oncologica ha dato grande impulso allo sviluppo di terapie combinate che agiscano sinergicamente, potenziando efficacia e selettività del trattamento. In particolare, la terapia fotodinamica rappresenta un approccio innovativo che, in combinazione con farmaci chemioterapici, ha dimostrato di ridurre l'incidenza di resistenza farmacologica e di aumentare l'efficacia terapeutica. Al fine di controllare e migliorare la biodisponibilità di più agenti terapeutici somministrati insieme, si ricorre alla progettazione e realizzazione di specifici nanosistemi biocompatibili e biodegradabili.

All'interno del microambiente tumorale si evidenziano delle caratteristiche peculiari, che permettono di discriminare le cellule cancerose dalle cellule sane: ipossia, acidosi, elevata concentrazione di perossido di idrogeno e glutatione. Sulla base di queste premesse, questo progetto di tesi ha riguardato la preparazione e caratterizzazione di cinque dimeri farmacologicamente inattivi di un chemioterapico, il paclitaxel (PTX), caratterizzati dalla presenza di diversi linker che, nelle condizioni redox dell'ambiente tumorale, vengono scissi e successivamente liberano il PTX. In seguito, tramite nanoprecipitazione sono state preparati due diversi nanosistemi:

- Dim₅_IR780@HSA: a base di albumina umana (HSA) contenente un dimero, che ha dimostrato agire anche come stabilizzante per la nanoparticella, in combinazione con un fotosensibilizzante, IR780, per il trattamento bimodale foto- e chemioterapico del tumore;
- Dim₁₂@NPs: contenente un dimero del PTX, con una porzione altamente selettiva nei confronti dell'HSA endogena, Evans Blue troncata (tEB), e che, *in vivo*, forma dei nanocomplessi stabili con la proteina.

In particolare, Dim₅_IR780@HSA ha dimostrato la capacità di sviluppare ROS in seguito ad irraggiamento luminoso e di rilasciare gradualmente nel tempo il

farmaco attivo in condizioni ossidanti. Mentre, Dim₁₂@NPs, *in vitro*, si lega efficacemente all'HSA, sviluppando dei nanocomplessi stabili nel tempo.

ACRONYMS

DDS: Drug delivery system

DMAP: 4-dimethylaminopyridine

EB: Evans Blue

ECM: Extracellular matrix

EPR: Enhanced Permeability and Retention

FBS: Fetal Serum Bovine

GSH: Glutathione

HSA: Human Serum Albumin

NPs: Nanoparticles

PBS: Phosphate-buffer saline

PDI: Polydispersity index

PDT: Photodynamic therapy

PS: Photosensitizer

PTX: Paclitaxel

ROS: Reactive oxygen species

SDT: Sonodynamic therapy

t-EB: Truncated Evans Blue

TME: Tumor microenvironment

INDEX

1. INTRODUCTION	3
1.1. Cancer	3
1.1.1. Tumor Microenvironment (TME)	3
1.1.2. Cancer Treatment	5
1.2. Chemotherapy and Paclitaxel	6
1.2.1. Paclitaxel structure and mechanism of action	6
1.2.2. Paclitaxel Bioresponsive prodrugs	8
1.3. Combination Therapy	9
1.3.1. Photodynamic therapy and IR780	10
1.3.2. IR780 structure and mechanism of action	11
1.4. Drug Delivery System	12
1.4.1. Albumin	13
1.4.2. Exogenous Albumin as drug carrier	15
1.4.3. Endogenous Albumin as potential drug carrier	15
2. AIM OF THESIS	17
3. RESULTS AND DISCUSSION	19
3.1 Paclitaxel prodrugs	19
3.1.1. Synthesis of PTX dimers	20
3.1.2. NMR Spectroscopic characterization of PTX dimers	23
3.2. HSA-based nanoparticles	24

3.2.1.	Exogenous HSA-based nanoparticles	25
3.2.2.	Prodrug-based nanoparticles	26
3.3.	Stability of NPs	26
3.3.1.	Stability of Dim ₅ @HSA	26
3.3.2.	Stability of Dim ₅ _IR780@HSA	28
3.3.3.	Stability of Dim ₁₂ @NPs	29
3.4	Reactive oxygen species production	31
3.5.	<i>In vitro</i> drug release profiles	32
4.	CONCLUSION	35
5.	EXPERIMENTAL SECTION	37
5.1.	Experimental procedure	37
5.2.	Preparation of nanoparticles	44
5.3.	Stability of NPs	44
5.4.	<i>In vitro</i> drug release profile	45
5.5.	Reactive oxygen species production	45
6.	BIBLIOGRAPHY	46

1. INTRODUCTION

1.1. Cancer

Cancer represents one of the leading causes of human death worldwide. The International Agency for Research on Cancer estimated 19.3 million new cancer cases and almost 10 million deaths occurred in 2020.¹

Cancer is an extremely complex and heterogeneous pathology, characterized by the uncontrolled growth and spread of cancer cells, due to dysregulation or disruption of different physiological pathways, resulting in tumor formation.

Cancer research involves several complementary scientific areas (i.e., medicinal chemistry, biology, toxicology, biomedical engineering, etc.), which aim at finding innovative and decisive strategies to tackle cancer progression.

1.1.1. Tumor Microenvironment

The tumor microenvironment (TME) is composed of a complexed and disordered blood vessels architecture, an increased extracellular matrix (ECM) and different cell types, including cancer, endothelial and immune cells, and fibroblasts.² In particular, endothelial cells provide the nutritional supply for mass growth; immune cells³, i.e., tumor-infiltrating B cells, have been proven to contribute to tumor progression; and, finally, cancer-associated fibroblasts promote cancer cells migration and metastasis invasion from the primary site into the surrounding tissues.

ECM is a three-dimensional network, typically composed of proteoglycans and fibrous or structural proteins (such as collagen, elastin, fibronectin, etc.), that supports cell division,⁴ and influences cancer cells migration by modulating its physico-chemical properties. Moreover, ECM gradient and concentration strictly regulate the migration speed of cancer cells through bloodstream. ECM proteins have been shown to act as a physical barrier, hampering drug delivery to cancer cells. Notably, ECM plays a key role in modulating immune cell recruitment, hence, potential immunotherapeutic strategies could be hindered by dysregulated ECM components.⁵

Due to the altered and enhanced metabolic pathways of cancer cells, TME shows peculiar hallmarks, such as acidosis and hypoxia, as well as high intracellular concentration of glutathione (GSH) and H₂O₂.

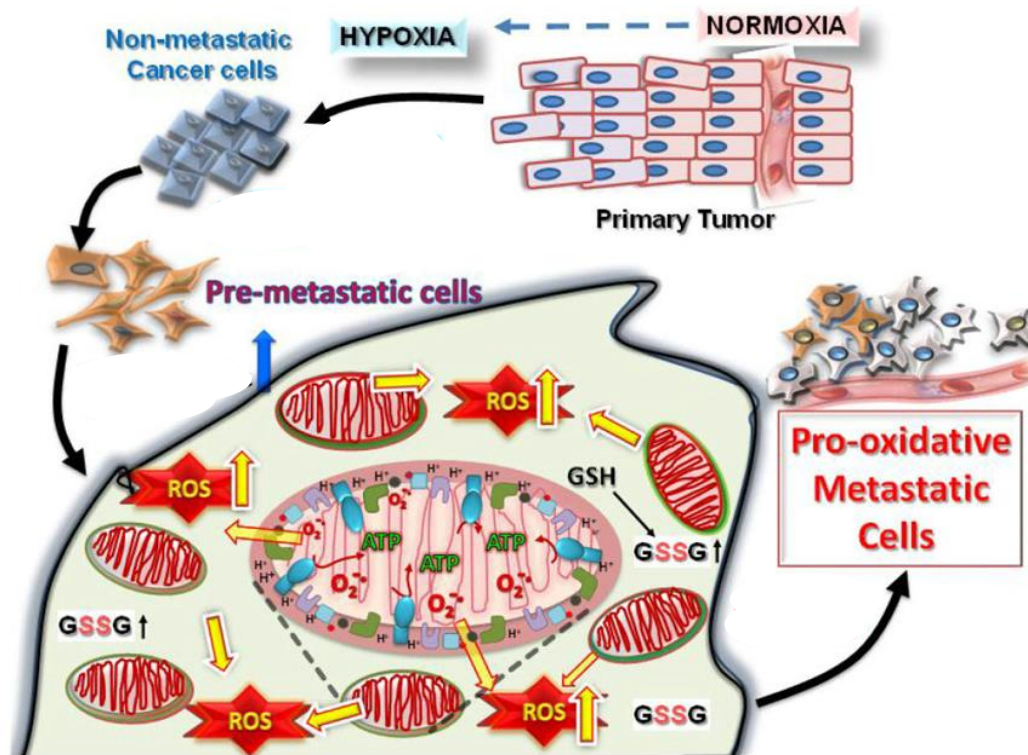


Figure 1 The changes occurring within the tumor microenvironment during the progression of malignant states.⁶

- **Acidosis:** in physiological conditions, the pH of human cells, blood vessels and extracellular environment, ranges between 7.35 to 7.45,⁷ while in cancer cells is around of 6.4–6.8,⁸ which mainly results from abnormal glucose metabolism, leading to a large production of lactate along with excess protons and CO₂.
- **Hypoxia:** most tumors show an imbalance between enhanced oxygen consumption by cancer cells and insufficient oxygen delivery from the bloodstream, due to the incomplete and disorganized tumor vessels (<20 mmHg O₂ pressure).⁹ Hypoxia promotes angiogenesis, suppression of immune reactivity and the generation of reactive oxygen species (ROS), and further induces metastasis formation and dissemination, reducing the effectiveness of many anticancer therapies, such as chemotherapy, photodynamic therapy (PDT) and sonodynamic therapy (SDT).
- **Increased TME levels of GSH and ROS:** TME is mainly controlled by the reduction and oxidation states of dihydronicotinamide-adenine dinucleotide phosphate (NADPH/NADP⁺) and GSH/GSSG. GSH is one of the most important antioxidants in the organism, regulating protein synthesis, DNA repair and, at molecular level, the cellular reducing environment.

NADPH, the reduced form of NADP⁺, is an essential reductive coenzyme for different cell growth and proliferation pathways, including GSH/GSSG recycling¹⁰. In particular, two molecules of GSH are oxidized by glutathione peroxidase to GSSG and then GSH is regenerated from GSSG by glutathione reductase. At the same time, NADPH and peroxides are consumed during these processes. The concentration of GSH in the extracellular environment is approximately 2 -20 μ M, instead in the TME, GSH levels are almost 4-fold higher than in healthy tissues, ranging between 2 to 10 mM.⁸ Over past decades, mounting evidence revealed that cancer cells produce a higher amount of ROS compared to their health counterparts, leading to an imbalance of redox condition. In particular cancer cells showed increased generation rate of H₂O₂ (up to 0.5 nmol/10⁴ cells/h).¹¹

Therefore, the typical TME hallmarks, could be exploited to improve the selectivity of antitumor therapeutics towards cancer cells.

1.1.2. Cancer Treatment

Surgery, radiotherapy, chemotherapy, hormone therapy and recently immunotherapy, alone or in combination, represent the current mainstream approaches for treating cancer. Briefly, surgery is the most effective treatment for solid tumors, eradicating the entire or partial tumor burden from the body, such as mastectomy, neurosurgery and prostatectomy.¹² However, in the presence of metastasis, tumor surgical removal could trigger an inflammatory response, leading to an accelerated growth of residual micrometastasis¹³. On the other hand, radiotherapy exploits high doses of ionizing radiation (i.e., x-rays), which induces cancer cell death by damaging DNA¹¹. Finally, hormone therapy is used for treating hormone-dependent tumors, i.e., breast, ovarian, endometrium, and prostate cancer, resulting in the inhibition of a specific hormone production or activity, leading to cell death.¹⁴

In recent years, immunotherapy has represented a relatively new approach, aimed at harnessing and selectively enhancing the host immune response toward cancer cells. The biological targets of immunotherapy mainly consist of the pathways involved in the regulation and proliferation of T cells, in order to restore the immunosurveillance.¹⁵ Due to its limited effectiveness as monotherapy, immunotherapy is combined with other approaches (chemotherapy, radiotherapy,

PDT). Notably, mounting evidence has shown that some chemotherapeutic drugs, such as doxorubicin (DOX) and paclitaxel (PTX), could also stimulate the immune response, leading to the immunogenic cell death (ICD).¹⁶

Unfortunately, standard approaches have revealed several limitations, including unfavourable pharmacokinetics profiles, poor bioavailability, immunodepression, non-selective biodistribution and induction of resistance phenomena.

1.2. Chemotherapy and Paclitaxel

Chemotherapy represents the standard first-line of treatment for different kind of cancers, depending on type, location and spreading. Among chemotherapeutics, Taxol®, the clinical formulation of paclitaxel (PTX), is considered one of the most widely used and effective antineoplastic agents. It was approved by the Food and Drug Administration (FDA) in 1992 for the treatment of ovarian, breast and lung cancer and for AIDS related Kaposi's sarcoma.¹⁷

PTX was first isolated from the bark of the pacific yew (*Taxus brevifolia*).¹⁸ However, due to the high complexity of total synthesis, the low extraction yield, the elevated ecological cost to produce a significant amount of PTX, a semisynthetic process has been developed, allowing to obtain PTX from 10-deacetylbaccatin III, a precursor extracted from European badger needles, *Taxus Baccata*.

1.2.1. Paclitaxel structure and mechanism of action

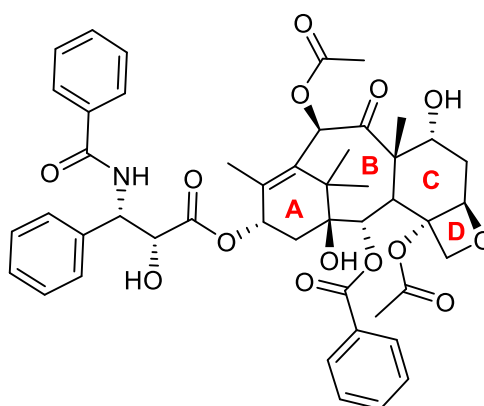


Figure 2 Structure of Paclitaxel

PTX is a diterpenoid belonging to the class of taxanes. It consists of a tetracyclic core (baccatin III), where rings are two cyclohexenes (A and C), a cyclooctane (B), and an oxetane (D), and a linear chain (N-benzoyl-β-phenyl-isoserine). The excellent anticancer activity of PTX is related to its different functional groups, such as the carbonyl group on C9 position, the acetyl group at C10 and the OH groups

at the C2' and C7 positions, which plays an important role in its reactivity. Due to its poor water solubility (0.3 $\mu\text{g/mL}$), PTX was administered in a mixture of 1:1 (v/v) cremophor EL and ethanol. However, cremophor EL is associated with severe side effects including hypersensitivity reactions, hyperlipidaemia, abnormal lipoprotein patterns, aggregation of erythrocytes and peripheral neuropathy. Therefore, numerous attempts were made to develop a water-based formulation of PTX. Conversely, PTX is soluble in organic solvents, such as dichloromethane (25 mg/mL), dimethyl sulfoxide (50 mg/mL) and methanol (45 mg/mL). In methanolic solution, it is not stable and, after two weeks at room temperature, it undergoes hydrolysis and transesterification.¹⁹

Mechanism of action. PTX binds microtubules during cell division, leading to the arrest of mitosis at G2/M cell phase and to apoptosis. Microtubules are the major components of the cytoskeleton, formed by heterodimers of two globular polypeptides, α - and β -tubulin. The simultaneous coexistence of polymerization and depolymerization processes of microtubules, known as 'dynamic instability', allows cells to rapidly reorganize the cytoskeleton and to drive the correct cell division. The predominance of one of the two phenomena is strictly regulated by the levels of free heterodimers into cytoplasm.

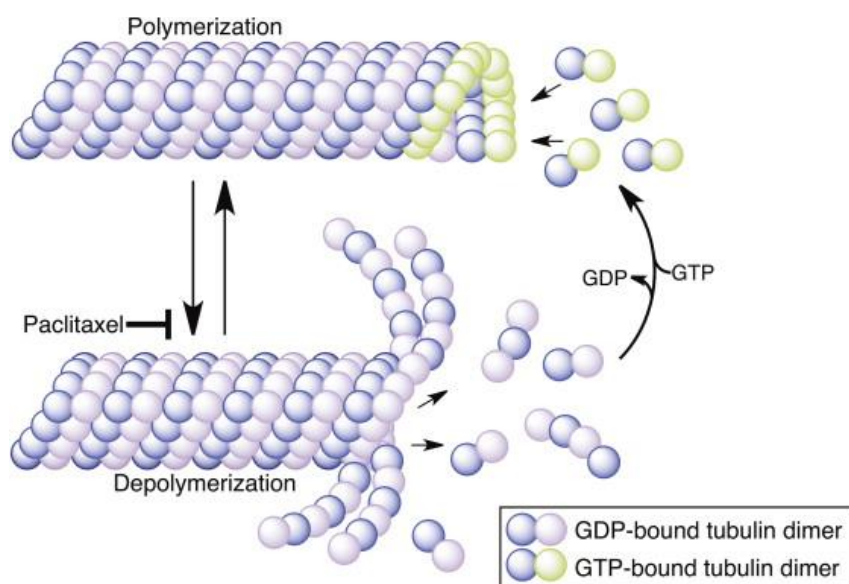


Figure 3 Paclitaxel stabilizes the microtubule by stopping depolymerization process and altering the dynamic instability

As shown in Figure 3, guanosine triphosphate (GTP)-bound tubulin dimers are incorporated at the end of the microtubule, forming a stabilizing cap. Following the GTP hydrolysis in GDP, tubulin subunit changes conformations, leading to the loss of the GTP-tubulin cap and to the consequent depolymerization. PTX acts suppressing depolymerization and, consequently, the dynamic instability.²⁰

1.2.2. Paclitaxel Bioresponsive Prodrugs

Prodrugs are very effective and promising alternatives to overcome issues related to the poor solubility of therapeutics and to the unfavourable pharmacokinetic and pharmacodynamic profiles. Prodrugs are pharmacologically inactive entities, whose activity was restored following enzymatic or biochemical transformations²¹.

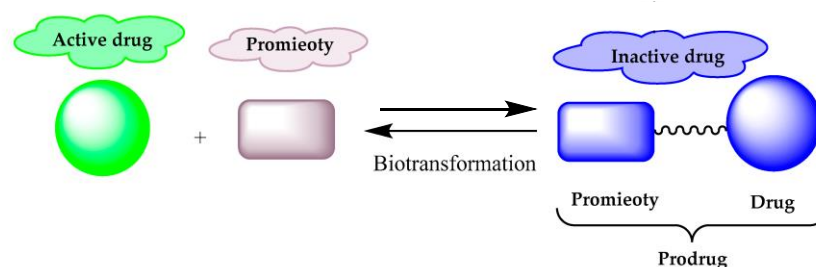


Figure 4 Schematic representation of conventional prodrug mechanism of action.

Thanks to the unique features of TME (i.e., pH, hypoxic and redox conditions) the design and synthesis of selective tumor-responsive prodrugs represent a promising approach for improving drugs' biodistribution and efficacy, as well as reducing the systemic toxicity.

Over the past decades, several PTX prodrugs have been widely investigated by introducing cleavable linkers at C2' or C7 positions.²² Notably, dimers, obtained through the conjugation of two PTX molecules via suitable chemical spacers, have gained increasing attention.²³

Among cleavable linkers, disulfide bridge (energy bond = 268 kJ/mol) represents a promising candidate, due to its reactivity in redox environment, indeed it can be easily broken down by reducing GSH into sulfhydryl groups, causing the degradation of prodrugs and the release of pharmacologically active molecule.^{10,21} In addition, the disulfide linker allows to achieve two key objectives: (i) high stability in blood circulation, avoiding the premature drug release, and (ii) the selective drug release into cancer cells.

Recent studies have described two speculative drug release mechanisms of disulfide bound in acidic condition, via enzymatic reaction or via hydrolysis, respectively (Figure 5).^{24,25} Initially, an intracellular deprotonated thiol, such as Cys-S⁻ or GS⁻, would attack the disulfide bond on the prodrug (I) to give the protonated or non-protonated intermediates (II, IV) and the thiol-cysteine adduct (III). Then, IV may preferentially undergoes cyclization reaction to give the free drug, VI in which thiolate anion moiety of substrate IV reacts with its adjacent

carbonyl group. Alternatively, the cyclization and subsequent decarboxylation give the final product **VI**. Following disulfide exchange reaction, the compound **III** can be reduced into anion **V**, via a nucleophilic attack of deprotonated thiol. Finally, compound **VII** is obtained through the cyclization or hydrolysis of **III**, catalysed by abundant hydrolytic enzymes or weak acidity in TME.

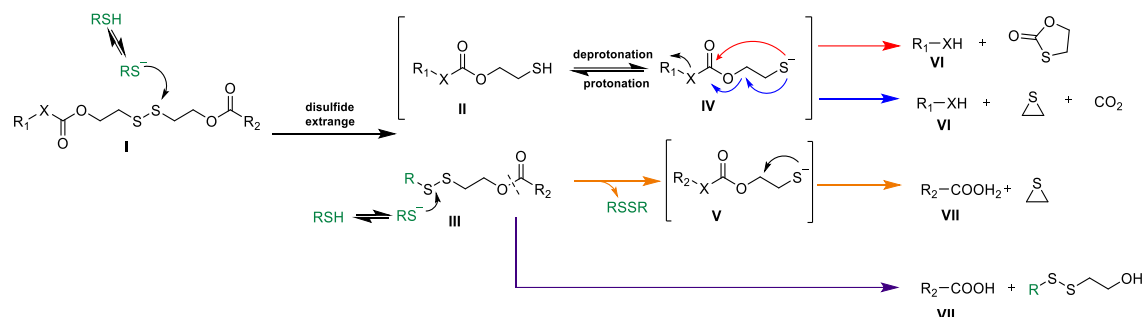


Figure 5 Two possible drug release mechanisms of disulfide-containing prodrugs.

Wang et al.²³ designed four kinds of PTX dimeric prodrug with different spacers, including mono-thioether, disulfide with one methylene, and disulfide with two methylene and ester, and explored the differences in redox responsiveness and antitumor activity. They confirmed that S-S bound is the most sensitive to reducing conditions, while mono-thioether is the most responsive to oxidizing species, in addition to the type of bond, the length of the carbon chain also play a crucial role in the redox-response. Therefore, they formed nanoparticles from PTX dimers because they can self-assemble into stable and uniformly sized nanoparticle around 200 nm. These findings suggested that PTX dimers in aqueous solution may self-rearrange, leading to the formation of stable nanoparticles (Figure 6).

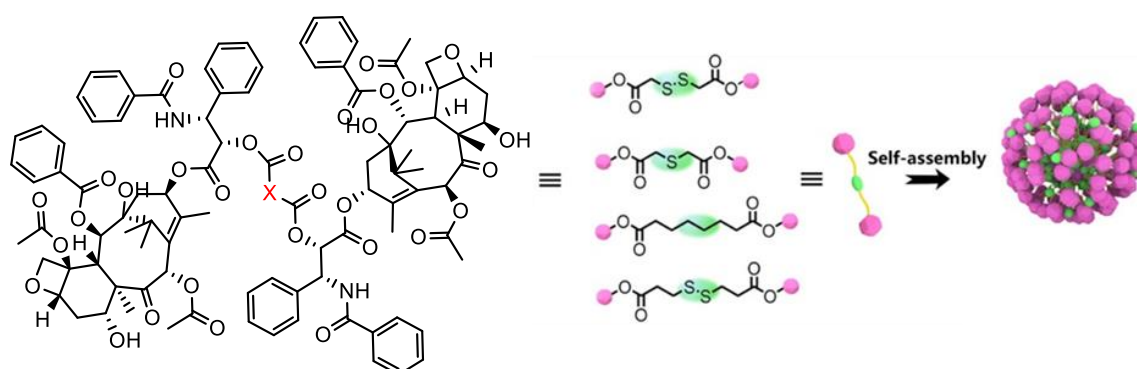


Figure 6 Self-assembly mechanism of four different Linker-Bridged prodrug nanoparticles.²³

1.3. Combination Therapy

As mentioned above, conventional cancer treatment exhibits many drawbacks, such as poor selectivity, systemic toxicity, as well as the development of resistance and recurrence phenomena. Therefore, an effective cancer therapy is still

challenging. Enormous efforts have been dedicated to developing suitably designed and personalized approaches.

Although monotherapy remains a widely used anticancer treatment, the bimodal regimens, combining photo- and chemo-therapy, represent a very appealing approach, to overcome multidrug resistance and to synergistically target different pathways.

1.3.1. Photodynamic Therapy

In 1970, the use of photodynamic therapy (PDT) has emerged as a valuable light-triggered treatment modality for the management of neoplastic and other malignant diseases.²⁶ PDT is already a successful and clinically approved therapeutic approach, which uses three key components: a photosensitizer (PS), light, and molecular oxygen. At an appropriate wavelength, light activates PS, which transfers its excited-state energy to molecular oxygen, inducing ROS generation and consequent apoptosis and/or necrosis of malignant cells.

In details, a PS in the ground state is characterized by paired electrons with a total spin of $S=0$ and a spin multiplicity of 1. As reported in Figure 7, upon the absorption of a light quantum with the appropriate energy ($\lambda=600-800$ nm), one electron is shifted to a previously unoccupied orbital (1PS) of higher energy. Since the ground state is energetically favoured over the excited states, the system will return rapidly to the 0PS state through relaxation phenomena. This phenomenon can occur by several mechanisms: vibrational relaxation by molecular relaxation from 1PS energetic level to 0PS (fluorescence emission,) or by a radiative relaxation from 3PS energetic level to 0PS (phosphorescence emission) or by heat dissipation (internal conversion, IC); intersystem crossing (ISC), non-radiative process, where, from 1PS the molecule may cross to an isoenergetic level of the triplet state, 3PS , where two electrons are unpaired and have the same spin (Figure 7).²⁷

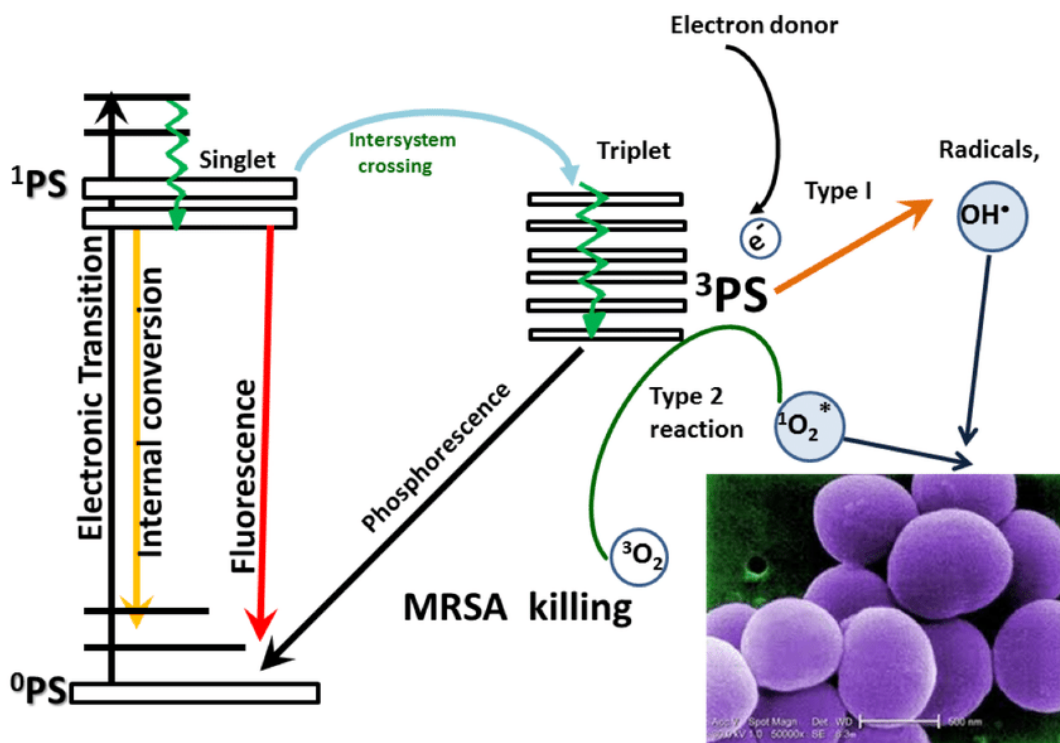


Figure 7 Jablonski energy diagram showing the mechanisms of PDT.²⁸

Moreover, the triplet-associated can be released via two competing pathways, type-I and type-II photochemical reactions:

- Type I reaction: electrons transfer takes place between the excited PS and a biological substrate, yielding free radicals, that further react with molecular oxygen to generate ROS (H_2O_2 , $\cdot\text{O}_2^-$, $\text{OH}\cdot$).²⁷
- Type II reaction: the PS in its triplet state can react directly with molecular oxygen and the energy (not electrons) transfer produces the cytotoxic reactive singlet oxygen ($^1\text{O}_2$).⁹

Several factors, including PS type, light dose, PS subcellular localization, play a crucial role in the type of cell death mechanism and in the effectiveness of therapy.²⁹

1.3.2. IR780 structure and mechanism of action

Among photosensitizers, IR780 iodide, a near-infrared dye, has shown wide applications both in PDT and in photothermal therapy (PTT), and as imaging agent in diagnostic (Figure 8).³⁰ This hydrophobic cation belongs to cyanine family and has absorption and emission maxima in the near-infrared (NIR) range, around 780 and 830 nm, respectively.³¹

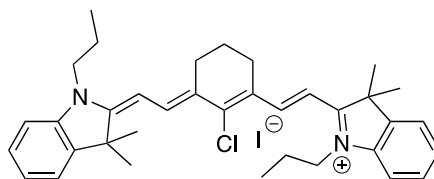


Figure 8 Molecular structure of IR780 iodide

IR780 has a rigid cyclohexenyl ring on the heptamethine chain, which results in poor water solubility, limiting its clinical use. It showed a low maximal tolerance dose of 1.5 mg/kg in mice. In this regard, IR780 is usually encapsulated within different types of nanostructures, in order to improve its bioavailability and to simultaneously decrease its toxicity.³²

Besides its strong NIR absorption, IR780 showed a high intensity of fluorescence and a remarkable photothermal conversion efficiency, which made it an excellent imaging dye for *in vivo* tumor tracking and a good photothermal. It is worth noting that, due to its lipophilicity, IR780 preferentially accumulate at the tumor site.

Moreover, Zheng et al.³³ investigated also the efficacy of IR780 as a sonosensitizing agent in the treatment of breast cancer. Specifically, they showed that SDT with IR-780 significantly inhibited the tumor growth with increased apoptosis and necrosis.

Finally, Jiang et al. encapsulated IR780 within human serum albumin (HSA) nanoparticles, to improve its bioavailability, and demonstrated that the nanoformulation severely inhibited tumor growth both *in vitro* and *in vivo*, by inducing ROS production as well as generating the hyperthermic effect.³¹

1.4. Drug delivery systems (DDS)

To improve pharmacodynamic and pharmacokinetic drug profile, the development of innovative and selective drug delivery systems (DDS) still represents a stimulating challenge in cancer therapy. In particular, nanocarriers (micelles, liposomes, nanoparticles etc.) have been extensively investigated in order to improve drugs selectivity and solubility, and to reduce potential toxicity and side effects.^{10,17} Nanoparticles, ranging to 100 nm, exploited the EPR effect (Enhanced Permeability and Retention), for increasing drugs effective concentration into tumor site, by using smaller quantities of therapeutics (Figure 9).

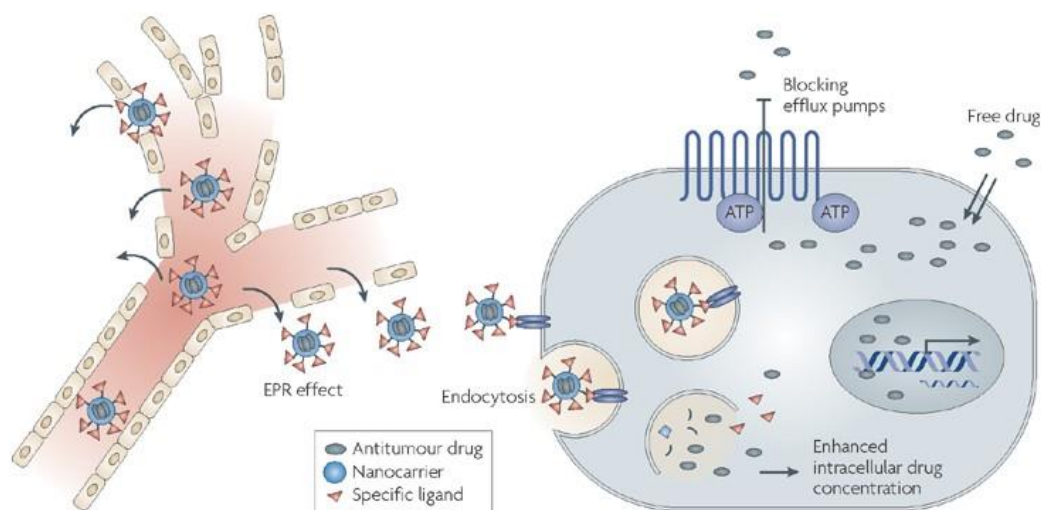


Figure 9 Illustration of EPR effect.³⁴

Indeed, due to the proliferation and uncontrolled growth of the tumor mass, blood vessels are incomplete and have fenestrations, while the lymphatic drainage system is completely absent. These characteristics of TME favour the accumulation of molecules, whose size is less than 200 nm, in order to improve the selectivity for tumor tissues compared to the healthy ones.³⁴

Furthermore, DDS allow to simultaneously vehiculate different drugs at the desired site for a multi-modal, synergistic approach, aimed at preventing metastasis dissemination and cancer recurrence. For instance, Martella et. al. developed dual-modal keratin-based nanoparticles, loaded with PTX and a photosensitizer Chlorin-e6 (Ce6) for treating osteosarcoma. The results indicated that PTX and Ce6 act in additive manner, demonstrating a superior effect compared to singularly administered free drugs.³⁵

1.4.1. Albumin

A versatile studied biomaterial for DDS production is human serum albumin (HSA), the most abundant human protein in the blood. HSA is synthesized in liver by hepatocytes and achieves a molecular weight of ~67 kDa and a blood concentration of 35-50 mg/mL.³⁶ Albumin consists of three homologous domains. Each domain contains two sub-domains, which contains 4 and 6 α -helices, respectively. Moreover, HSA contains 35 cysteine residues of which 34 form intramolecular disulfide bridges, which contribute to its high stability. The availability of a free cysteine residue at position 34 (Cys34) for covalent attachment of drugs is an attractive feature, exploited in drug delivery.³⁷



Figure 10 Covalent conjugation of a drug to HSA via Cys34.³⁷

HSA has emerged as a natural carrier for a wide range of compounds both endogenous and exogenous within the organism. HSA, as nanocarrier, shows many advantages, i.e., biodegradability and biocompatibility, non-toxicity, non-immunogenicity, and it can be easily functionalized, by exploiting its chemical moieties (-NH₂, -COOH, -SH). In addition, HSA preferentially accumulates within tumor, due to several factors: (i) the ample need of the proliferating tumor mass to cover its amino acid supply by digesting albumin; (ii) the exploitation of the EPR effect; (iii) the presence of two albumin-binding proteins, the gp60 receptor on the tumor endothelium, and SPARC (Secreted Protein, Acidic and Rich in Cysteine), a secreted glycoprotein with high binding affinity to HSA in the tumor interstitium (Figure 11).³⁶

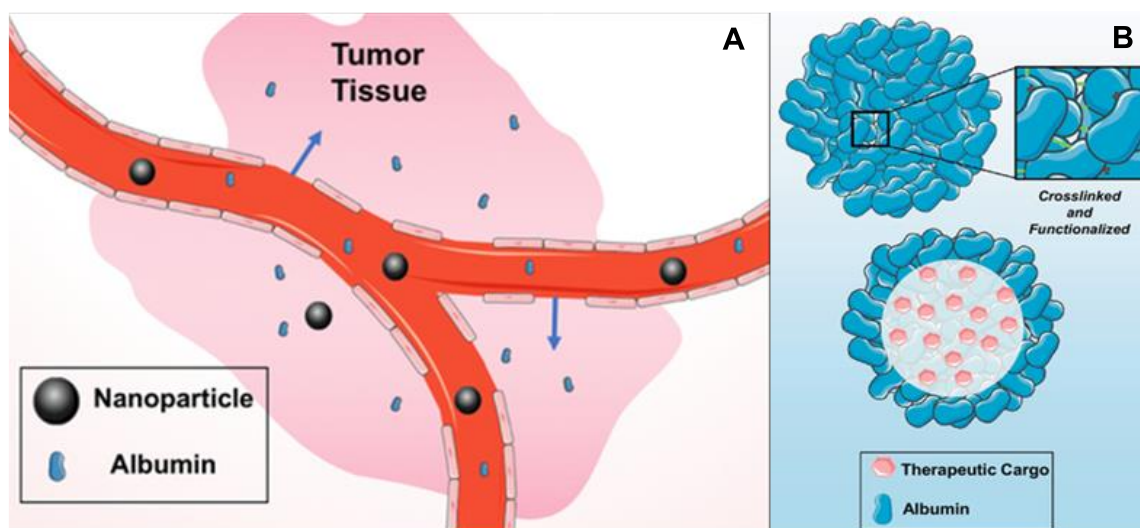


Figure 11 Schematic illustration of (A) accumulation of HSA in tumors and (B) HSA-based nanoparticles.³⁶

1.4.2. Exogenous albumin as a drug carrier

One of the most explored methods that use HSA as a carrier for anticancer therapies involves the encapsulation of drugs in exogenous HSA-based nanoparticles. This approach exploits the intrinsic properties of HSA, such as its long half-life, as well as its ability to load hydrophobic ligands and to deliver them into tumor.³⁶ HSA nanoparticles have been extensively investigated for treating different pathological conditions. In particular, HSA-based nanotechnology (nab-technology) was introduced as safe and effective formulation technique. In 2005, the FDA approved Abraxane®, an albumin-paclitaxel nanoparticle with an average size of 130 nm, for the treatment of metastatic breast cancer. Abraxane® improves PTX solubility and stability, avoiding the use of CrEL and reducing the related anaphylactic 19 reactions.³⁸ Similarly, Yu et al. successfully prepared gemcitabine (GEM)-loaded HSA by using the same technique for the treatment of drug-resistant pancreatic cancer.³⁹

1.4.3. Endogenous albumin as potential drug carrier

To achieve targeted drug delivery to tumor tissue using HSA as an endogenous drug carrier, it has proposed a macromolecular prodrug strategy: formation of a covalent bond between endogenous HSA and drugs. Indeed, CYS-34 from HSA represents the most abundant free thiol group in the blood, and competitive side reactions with other free thiols are not a significant concern because cysteines are typically found in unreactive disulfide bridges form. Kratz and colleagues used an approach based on the use of a maleimide hydrazone derivative of the cytotoxic drug doxorubicin (DOX) to form an *in situ* thioether covalently bonded with the CYS-34 (Figure 12).⁴⁰ An acid sensitive hydrazone linker is present in the structure to promote doxorubicin release triggered by the highly acidic environment of cancer cells lysosomes and endosomes.

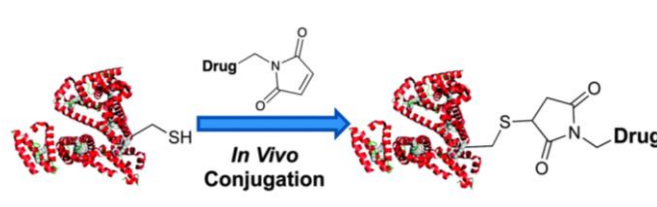


Figure 12 Endogenous Serum Albumin with Thiol-Binding drug.⁴¹

Another approach to promote *in situ* interaction with HSA involves the conjugation of therapeutic agents to ligands that naturally bind endogenous HSA in a non-covalent manner. A notable example of these small molecule binders is the dye

Evans Blue (EB), that exhibits selective and reversible binding to HSA. Since each HSA molecule can bind up to 14 EB molecules and owing to the abundance of HSA in the blood, almost all of the injected EB is retained in the blood after intravenous injection.⁴² Based on this, several analogues of EB have been reported in the literature in order to exploit its HSA affinity to selectively transport drugs. Since the chemical structure of EB is not favourable for derivatization, truncated versions of this molecule have been designed to maintain its HSA-binding capabilities but also to allow modifications such as conjugation with other drugs or imaging agents (Figure 13). Many derivatizations have been designed to replace one of the 1-amino-naphthol-2,4-disulfonic acid moieties with other molecules and generate truncated EB (tEB).⁴³

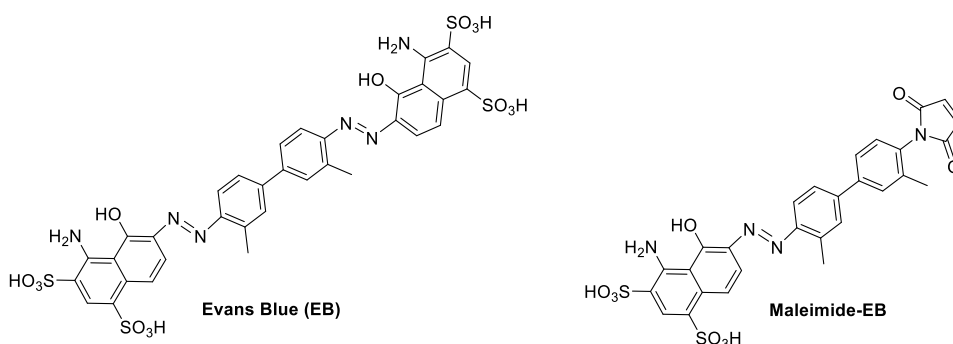


Figure 13 Chemical structures of Evans Blue (EB) and its derivative maleimide-tEB.⁴²

Therefore, an optimal strategy is to bind EB with prodrugs in order to generate albumin-prodrug nanocomplexes upon avid binding to endogenous HSA. For instance, Zhang et al. synthesised amphiphilic prodrug nanoparticles from a camptothecin prodrug bearing a redox responsive disulfide linker, CPT-ss-EB (Figure 14) that were then transformed to efficient albumin-based nanoparticles.⁴⁴

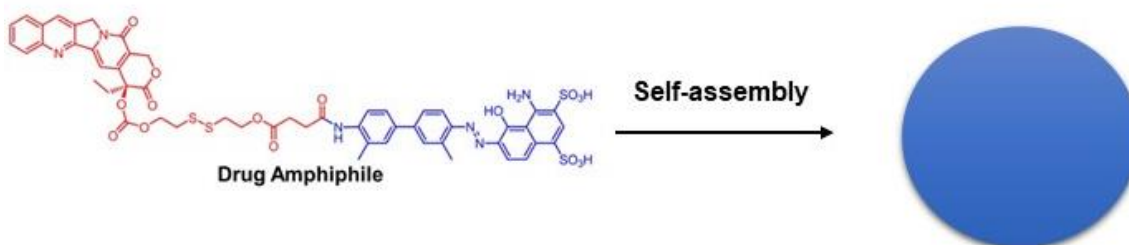


Figure 14 Self-assembly of CPT-SS-EB prodrug to form HSA-based NP.⁴⁴

2. AIM OF THESIS

The aim of this project is to synthesize and characterize different bioresponsive PTX prodrugs, (i) to be loaded in albumin (HSA)-based nanoparticles, in combination with the photosensitizer IR780, for bimodal anticancer therapy; or (ii) to self-assemble in water and being able to *in vivo* bind endogenous HSA. It is the most abundant blood protein and represents the natural carrier of hydrophobic endogenous and exogenous molecules. It is also a validated biomaterial for the transport of several drugs (e.g., Abraxane®): thanks to the EPR effect and the presence of two over-expressed albumin-binding proteins (gp60 receptor and SPARC), HSA preferentially accumulates at the tumor site.

To this purpose, five different dimers, **4**, **5**, **6**, **8**, **10**, **12** bearing different redox-responsive linkers, were synthesized and investigated (Figure 15).

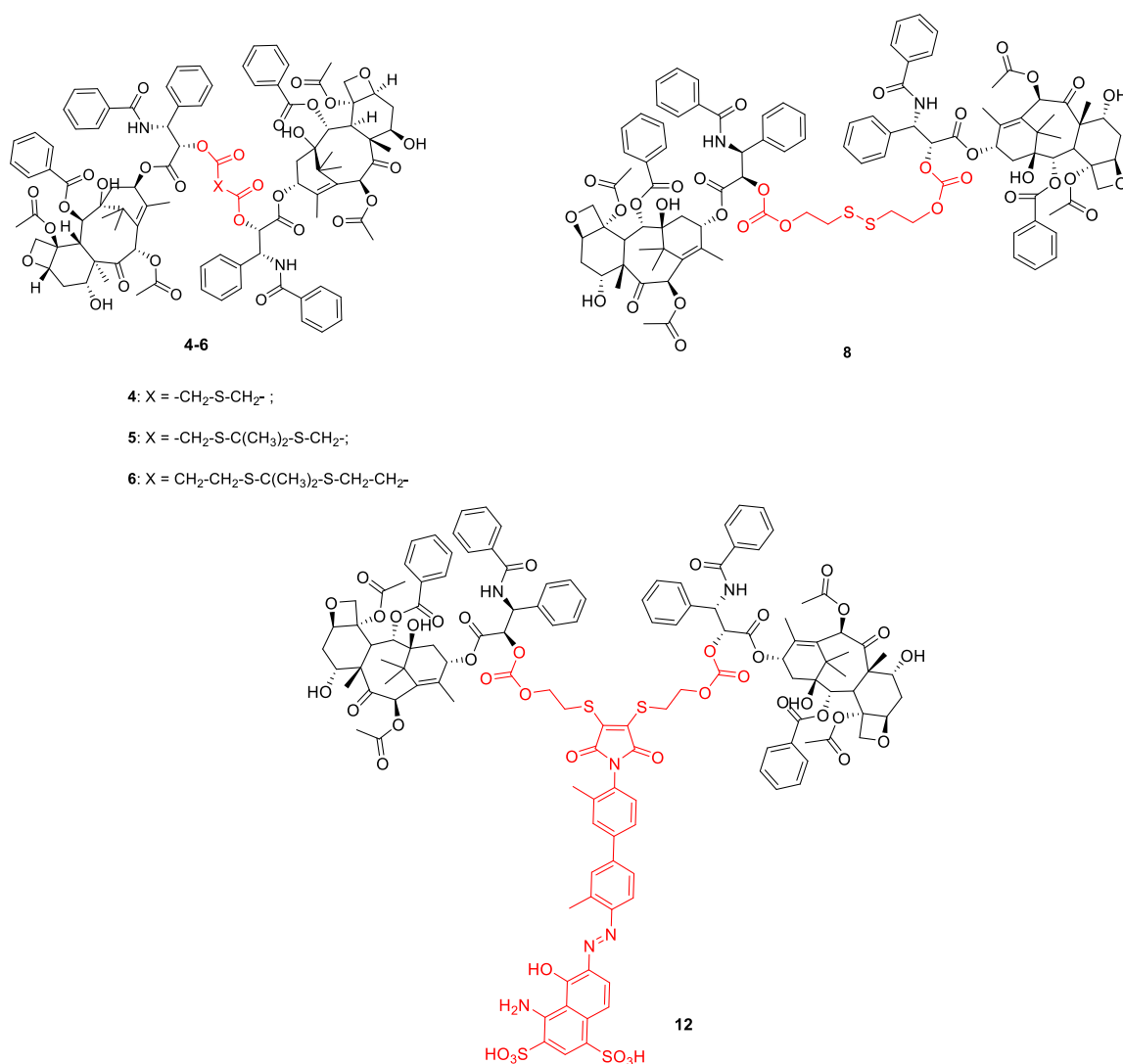


Figure 15 PTX dimers synthesised

The second aim of my project has been the development of selective nanocarriers based on PTX dimers. To this end, I investigated two approaches:

- a) the preparation of HSA-based nanoparticles loaded with the PTX dimer **5**, also in combination with IR780, Dim₅@HSA and Dim₅_IR780@HSA.
- b) the production of PTX dimer (**12**)-based nanoparticles, capable of *in vivo* binding endogenous HSA, thanks to the presence of tEB moiety, Dim₁₂@NPs.

All nanoparticles were obtained by nanoprecipitation and further characterised in terms of size and stability under different conditions (H₂O, PBS and PBS with 10% FBS, H₂O or PBS with BSA 35 mg/mL) using dynamic light scattering (DLS), ROS production and drug release profiles under different conditions (PBS, H₂O₂, dark, light) through HPLC analysis.

3. RESULTS AND DISCUSSION

3.1. Paclitaxel prodrugs

The thesis work aims to prepare and investigate five different dimers, **4**, **5**, **6**, **8** and **12**, bearing various redox-responsive linkers, for the controlled and selective drug release within tumor microenvironment (Figure 166).

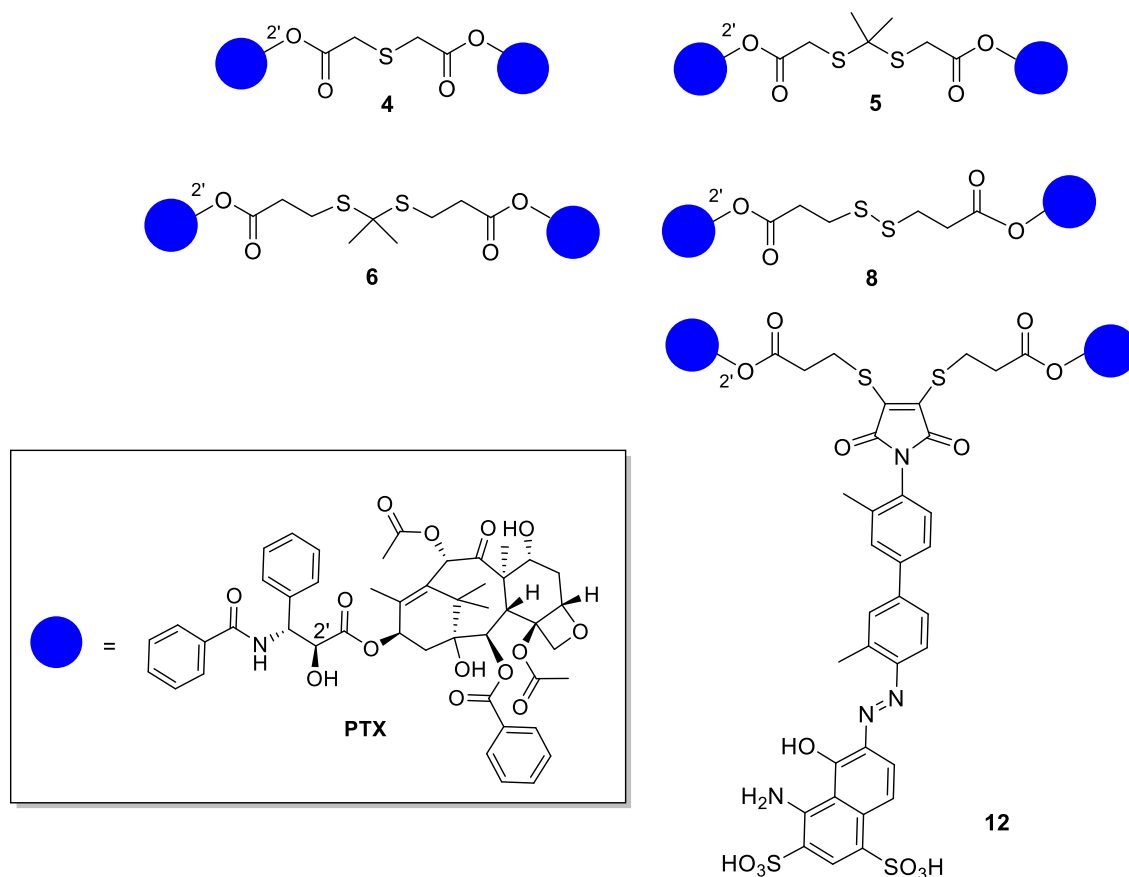


Figure 16 PTX dimers synthesised with different linkers

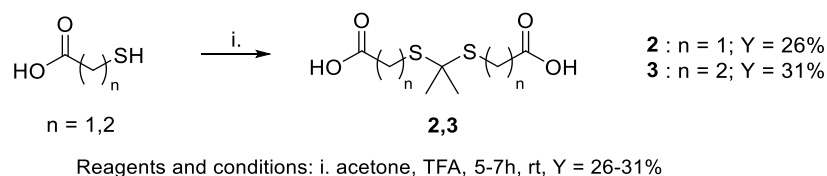
In a recent work,⁴⁵ Varchi and collaborators reported the preparation of bioresponsive nanoparticles assembled from compound **4**, bearing a thioether spacer,⁴⁶ and loaded with a photosensitizer (PS), Pheophorbide A, for bimodal treatment of solid tumors.⁴⁵ Briefly, the authors observed that, after exposure to TME-mimicked GSH or ROS concentrations, nanoparticles promptly disassembled, leading to drug release. Remarkably, nanoparticles exhibited a significant faster ROS-triggered release of PTX, conversely, a quite slow release under reductive conditions.

Moreover, Pei et al.⁴⁷ prepared also bimodal nanoparticles containing a PS and the dimer **6** and demonstrated that, upon light irradiation, the PS generated ROS species, triggering a massive PTX release. Therefore, I synthesized derivatives **5**,

bearing a shorter thioketal, and **8**,²³ with a disulphide bridge spacer, aimed at reaching a faster ROS-controlled release of PTX. Finally, to promote the interaction with endogenous HSA, I further synthesized compound **12**, bearing a truncated Evans Blue (tEB) pendant, that exhibits selective and reversible binding to HSA,⁴³ leading to the formation of small albumin/prodrug nanocomplexes.

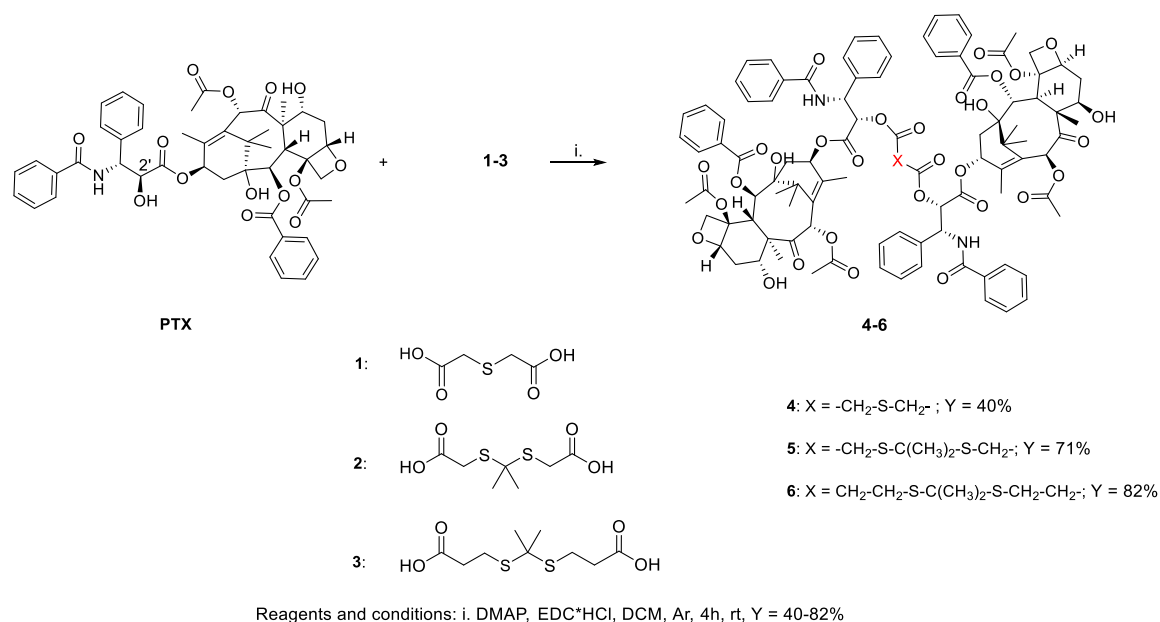
3.1.1 Synthesis of PTX dimers

The synthesis of PTX dimers (**4-6**) was achieved following a multi-step literature procedure.⁴⁸



Scheme 1 Synthesis of the dicarboxylic acids 2-3

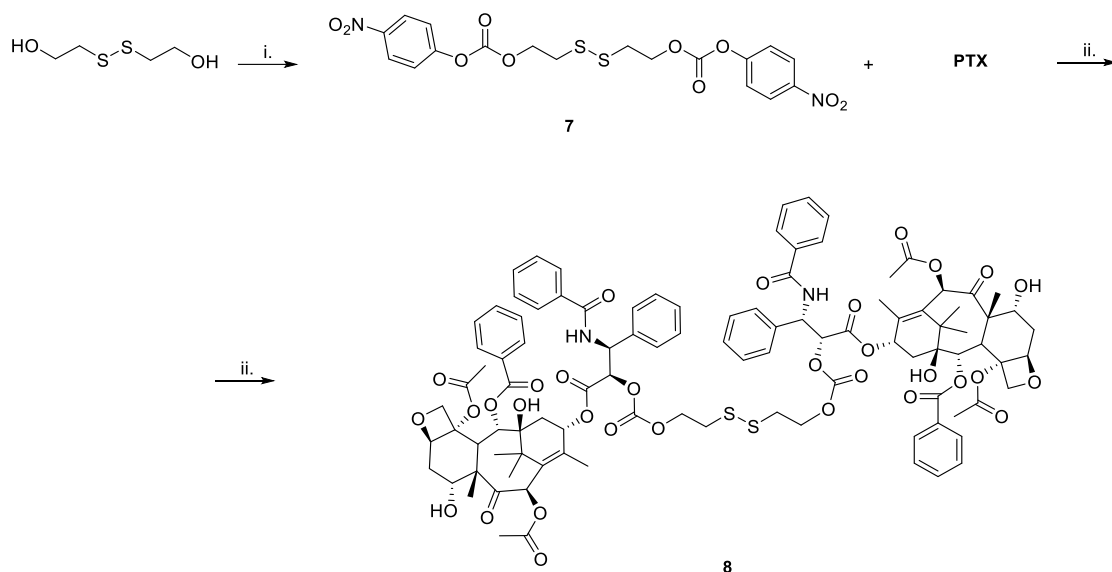
Scheme 1 outlines the synthesis of compounds **2** and **3**. Starting from a mixture of commercially available mercapto-acids (2-mercaptoacetic acid and 3-mercaptopropanoic acid), trifluoroacetic acid and acetone, the dicarboxylic acids **2-3** were obtained as white solids ($Y = 26\%$ and 31% , respectively). ¹H-NMR analysis showed following signals: -CH₃ signal at 1.04 ppm (singlet) and -CH₂ at 2.86 ppm (doublet) for compound **2**, while -CH₃ at 1.60 ppm (singlet) and -CH₂ at 2.68 ppm (doublet) and 2.91 ppm (doublet) for compound **3**.



Scheme 2 Synthesis of the PTX dimers 4-6

Subsequently, PTX was firstly dissolved in dichloromethane (DCM) and then treated with dicarboxylic acids (**1-3**) in presence of *N*-(3-dimethylaminopropyl)-*N'*-

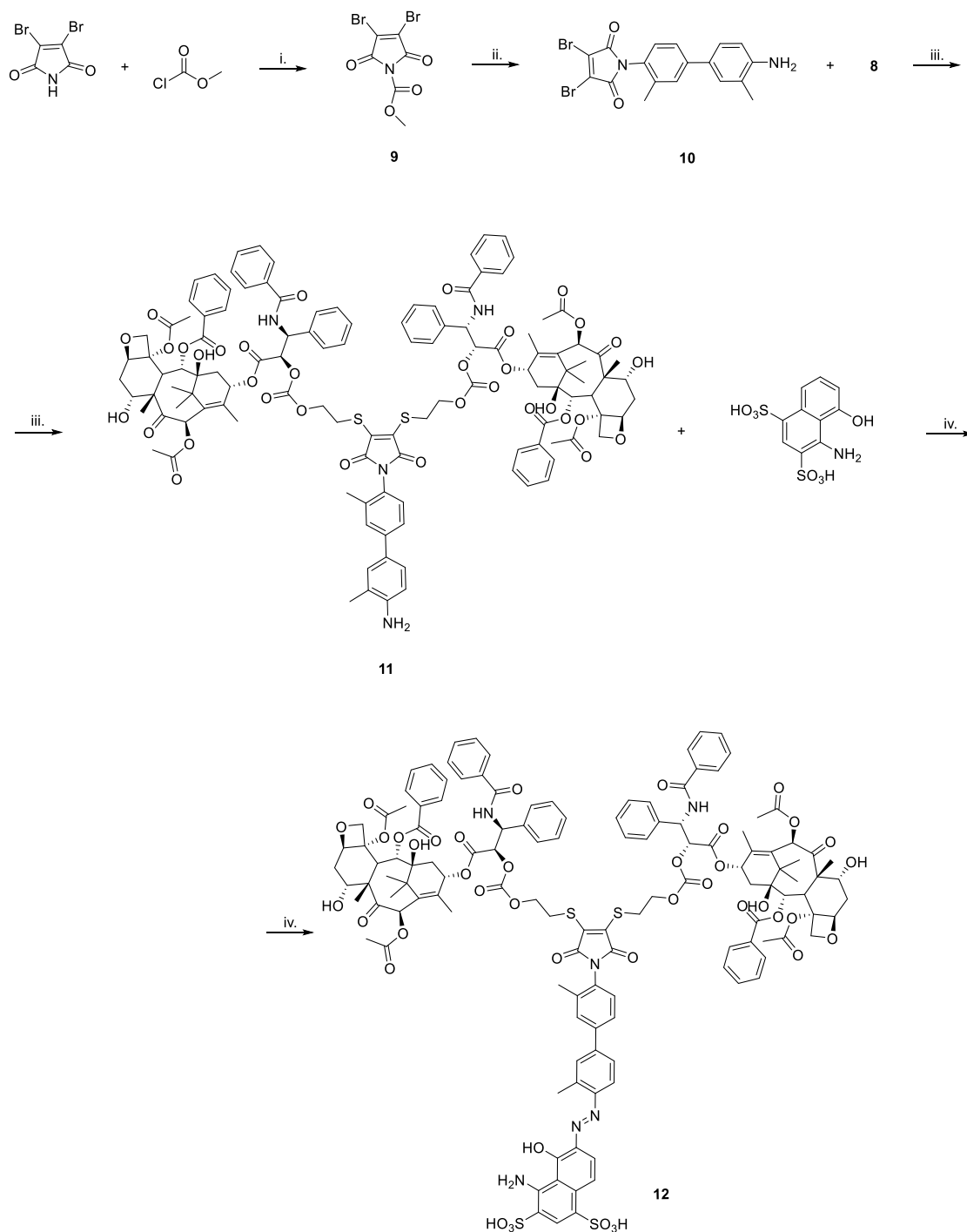
ethylcarbodiimide hydrochloride (EDC*HCl), as a carboxyl activating agent, and a catalytic amount of 4-dimethylaminopyridine (DMAP) to afford the desired dimers, **4-6**, through the esterification of 2'-OH moiety (Scheme 2).⁴⁷ This step allowed for easy recovery of unreacted starting material, PTX.



Reagents and conditions: i. *p*-nitrophenyl chloroformate, DIPEA, DCM, 5h, Y = >98%; ii. DMAP, EDC*HCl, DCM, Ar, 4h, rt, Y = 40%

Scheme 3 Synthesis of PTX dimer **8**

Dimer **8** was prepared in a two-step protocol, as depicted in Scheme 3. Bis(2-hydroxyethyl)disulfide was first activated by reacting with *p*-nitrophenyl chloroformate in presence of *N,N*-diisopropylethylamine (DIPEA), to obtain a white solid **7** in almost quantitative yield (Y = 98%). Compound **7** was then used as substrate for the subsequent formation of carbonate **8**. In details, **7** was dissolved in DCM and reacted with a catalytic amount of DMAP at room temperature under inert argon atmosphere.⁴⁹ The product was isolated and characterized through ¹H-NMR analysis (Y = 83%).



Reagents and conditions: i. 4-methylmorpholine, THF, 4h, rt, Y = 40%; ii. tolidine, DCM, N₂, 3h, rt, Y=83%; iii. TCEP-HCl, DMAP, DCM/THF, N₂, 2h, rt, Y=25%; iv. HCl, NaNO₂, H₂O, CH₃CN, NaHCO₃, 3h, rt, Y=50%.

Scheme 4 Synthesis of dimer 12

In order to obtain dimer **12**, bearing a selective albumin-binding *t*-EB pendant, we performed the synthesis of the *N*-tolidine-2,3-dibromomaleimide **10** (Scheme 4).⁵⁰ First, 2,3-dibromomaleimide has been activated by means the introduction of methoxycarbonyl group.⁵¹ In details, maleimide was treated with *N*-methylmorpholine and methyl chloroformate in THF at room temperature for 1 h. Compound **9** was obtained, as purple solid, in excellent yield (Y = 80%) and

characterized by $^1\text{H-NMR}$, without any further purification. Stirring N-methoxycarbonyldibromomaleimide (**9**) with *o*-tolidine, at room temperature, for 19 h under inert atmosphere, successfully afforded compound **10** (Y=83%). A slight excess of compound **10** was then reacted with dimer **8**, in presence of a large amount of DMAP and tris(2-carboxyethyl)phosphine hydrochloride (TCEP-HCl), as strong disulfide reducing agent, affording compound **11** (Y = 25%). Lastly, compound **12** was obtained through diazotization and following azo-coupling reactions. The diazonium salt was prepared by treating compound **11** with NaNO_2 , and HCl in acetonitrile, following the salt formation, the reaction mixture turned orange. Finally, 1-amino-8-naphthol-2,4-disulfonic acid dissolved in aqueous NaHCO_3 solution, was added to the mixture at 0 °C, yielding to crude diazo-compound **12**. Unfortunately, the compound resulted unstable on silica gel, therefore, to remove acetonitrile and undesired salts, the crude was first lyophilized and, once dissolved in H_2O , was further purified through dialysis bag (MWCO: 12 kDa), against $\text{H}_2\text{O}/\text{EtOH}$ 80:20 v/v.

3.1.2. NMR Spectroscopic characterization of PTX dimers

Figure 17 compares $^1\text{H-NMR}$ spectra of all synthesized prodrugs with PTX, evidencing the disappearance of the typical 2' OH singlet of PTX at 3.51 ppm.

In addition, it is worth noting:

- for compound **4**, the presence of thioether signals: $-\text{CH}_2$ at 3.16 (doublet) and 3.27 (doublet) ppm;
- for compound **5**, the presence of thioketal spacer signals: $-\text{CH}_2$ at 3.42 (doublet) and $-\text{CH}_3$ at 1.45 (singlet) ppm;
- for compound **6**, the presence of the longer thioketal spacer signals: two $-\text{CH}_2$ at 2.6-2.9 ppm (multiplet) and $-\text{CH}_3$ at 1.58 (singlet) ppm;
- for compound **8**, the presence of the disulfide spacer signals: two the $-\text{CH}_2$ at 2.88 (triplet) ppm and 4,31(triplet) ppm;
- for compound **12**, the presence of additional aromatic signals, due to the protons of both tolidine and tEB moieties.

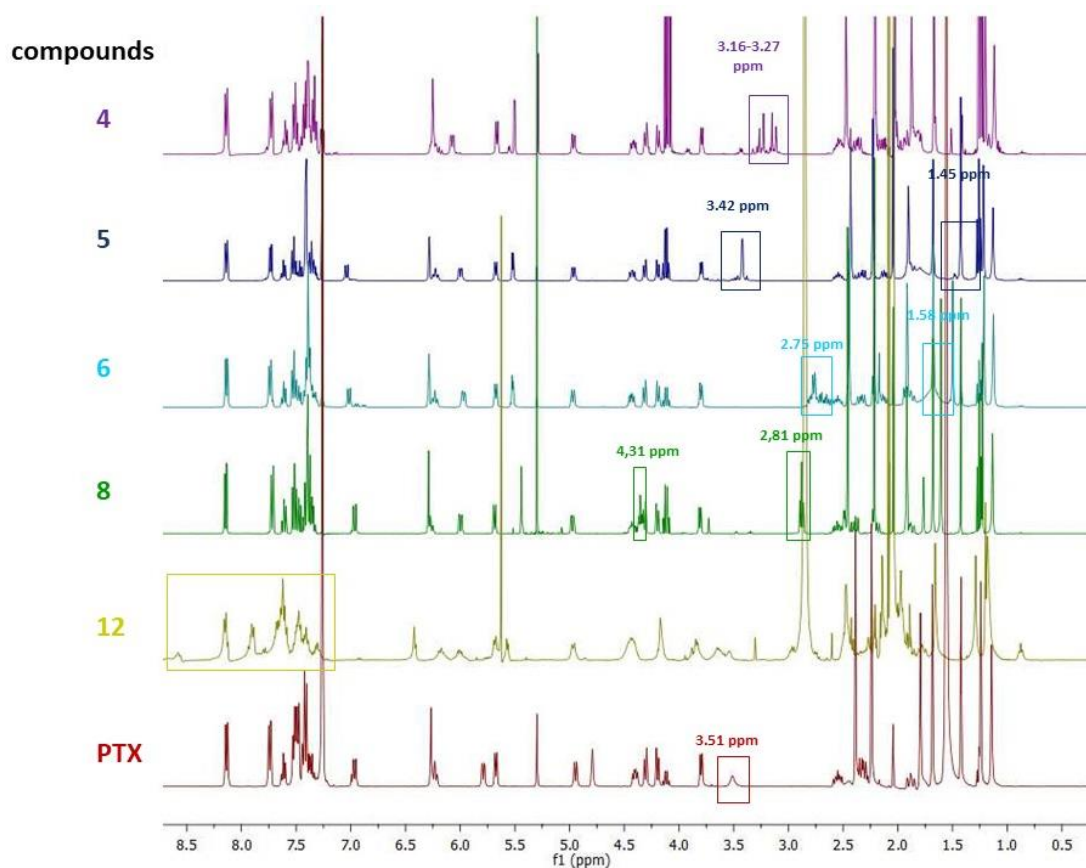


Figure 17 Comparison between ^1H NMR spectra of PTX (red line) and dimers **4** (purple line), **5** (blue line) and **6** (light blue line), **8** (green line) and **12** (yellow line) in CDCl_3 (400 MHz)

3.2 HSA-based nanoparticles

As mentioned above, PTX administration displayed several critical issues, mainly due to its extremely poor water solubility and elevated systemic toxicity.⁴⁶ Therefore, the second goal of my work has been the development of safer and selective nanocarrier based on PTX dimers. To this end, I explored two approaches: (i) the preparation of HSA-based nanoparticles loaded with PTX dimer **5** and IR780, (ii) and the production of PTX dimer (**12**)-based nanoparticles, capable of *in vivo* binding endogenous HSA, thanks to the presence of tEB moiety. To the best of my knowledge, PTX dimer bridged with ROS-responsive thioketal, **5**, has never been synthesized before, thus, we selected this prodrug for the encapsulation within HSA nanoparticles in combination with IR780, aimed at obtaining the PDT-triggered drug release.⁵²

In conclusion, I prepared two different nanoformulations:

- HSA-based nanoparticles, Dim₅_IR780@HSA and Dim₅@HSA;
- PTX dimer-based nanoparticles, Dim₁₂@NPs.

All NPs, were obtained by nanoprecipitation method,⁴⁶ and further characterized

in terms of hydrodynamic diameter (d), polydispersity index (PDI) and stability under different conditions (e.g., H₂O, PBS, PBS with 10% fetal bovine serum, FBS, BSA in H₂O or PBS) by using dynamic light scattering (DLS). This technique measures the intensity variation of light scattered by the sample as a function of time. Intensity variation measured by the detector is generated by the Brownian motion of the particles at the origin of the scattering. At the same temperature and viscosity, small particles move rapidly, creating rapid changes in scattering intensity, while large particles move slowly, creating slow changes in intensity. From the frequency of intensity variation, we obtain the dispersion coefficient. The Stokes-Einstein equation allows to convert the diffusion coefficient into a hydrodynamic diameter.

3.2.1 Exogenous HSA-based nanoparticles

PTX dimers in aqueous solution showed to self-rearrange, leading to the formation of stable nanoparticles. This phenomenon is mainly due to the introduction of a free rotatable σ -bond between two PTX molecules, which confers flexibility to the structure and inhibits the long-range growth and precipitation of PTX crystals.⁴⁶

Dim₅@HSA and Dim₅_IR780@HSA were obtained by exploiting nanoprecipitation procedure.⁵³

Briefly, 92 μ L of an ethanolic solution of **5** (10 mg/mL) were slowly added to an HSA aqueous solution (3.7 mg/mL), under vigorous stirring, affording Dim₅@HSA. The ethanolic mixture containing **5** (92 μ L, concentration 10 mg/mL) and 7% (w_{IR780}/w_{HSA}) of IR780 iodide (45 μ L, concentration 8 mg/mL), were slowly added to an HSA aqueous solution (3.7 mg/mL), under vigorous stirring, providing Dim₅_IR780@HSA.

The as-prepared NPs were analysed by DLS.

Table 1 DLS characterization of Dim₅@HSA and Dim₅_IR780@HSA

Sample	d (nm)	PDI
Dim ₅ @HSA	123.55	0.115
Dim ₅ _IR780@HSA	136.31	0.157

As reported in Table 1, Dim₅@HSA and Dim₅_IR780@HSA showed an average hydrodynamic diameter of 124 and 137 nm, respectively, and a good polydispersity index between 0.11 and 0.16, making them suitable for exploiting the EPR effect for preferential tumor accumulation.⁵⁴

3.2.2 Prodrug-based nanoparticles

Prodrug-based nanoparticles were prepared by nanoprecipitation procedure.⁴⁶ Briefly, 200 μ L of a DMSO solution of dimer **12** (15 mg/mL in DMSO), were added to 0.94 mL of milliQ H₂O or PBS (1 mg/mL) at room temperature under vigorous stirring. The as-obtained Dim₁₂@NPs were analysed by DLS.

Table 2 DLS characterization of Dim₁₂@NPs

Sample	Solvent	d (nm)	PDI
Dim ₁₂ @NPs	H ₂ O	70.98	0.252
	PBS	175.35	0.263

As shown in Table 2, Dim₁₂@NPs prepared in aqueous solution displayed a smaller hydrodynamic diameter than nanoparticles obtained in PBS, 70.98 vs. 175.35 nm, respectively, while both nanoformulations showed good and similar PDI values. Moreover, only Dim₁₂@NPs in H₂O were stable over time, conversely in saline solution, nanoparticles tended to aggregate.

3.3 Stability of NPs

3.3.1 Stability of Dim₅@HSA

The stability of Dim₅@HSA was evaluated at 37°C by performing DLS analysis at different time intervals (0, 3, 7, 24, 48, 72 and 96 h) and under three different conditions:

- H₂O;
- PBS at pH = 7.4;
- PBS + 10% FBS, to explore NPs behaviour in presence of serum proteins.

H₂O: As shown in Figure 18, Dim₅@HSA shown an excellent stability in aqueous solution and an optimal colloidal stability, thus, maintaining a constant average diameter above 130 nm over 96 h and PDI around 0.1.

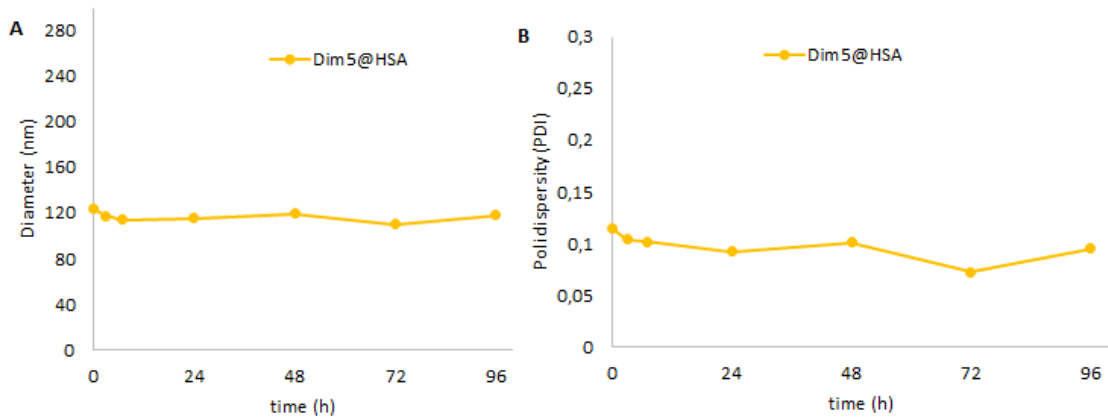


Figure 18 Stability of Dim₅@HSA in H₂O. (A) Diameter. (B) PDI

PBS at pH=7.4: Figure 19 showed the significant stability of Dim₅@HSA in PBS at 37°C, over 96 h, nanoparticles showed an average diameter of about 130 nm and PDI around 0.1.

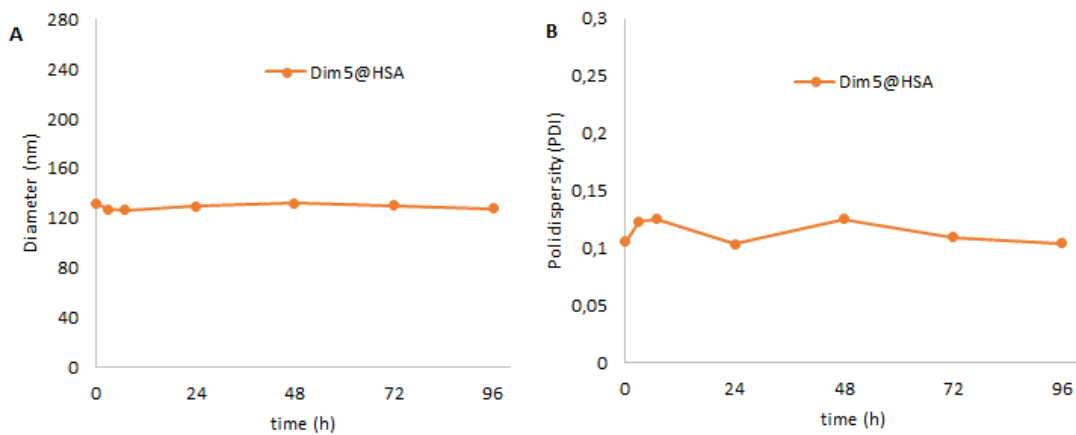


Figure 19 Stability of Dim₅@HSA in PBS. (A) Diameter. (B) PDI.

PBS with 10% FBS at pH=7.4: Under these conditions, after a slight increase in the first 24 hours, average hydrodynamic diameter remained constant, around 160 nm (Figure 20A). The PDI values (around 0.2) were very stable over the time (Figure 20 B).

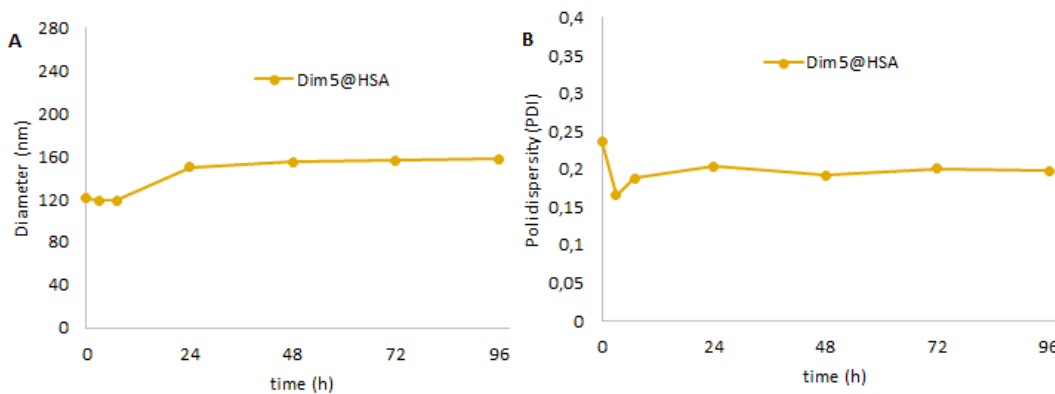


Figure 20 Stability of Dim₅@HSA in PBS with 10% FBS. (A) Diameter. (B) PDI.

3.3.2 Stability of Dim₅_IR780@HSA

The stability of Dim₅_IR780@HSA was evaluated at 37°C by performing DLS analysis at different time intervals (0, 3, 7, 24, 48, 72 and 96 h) and under the following conditions:

- H₂O;
- PBS at pH = 7.4;
- PBS + 10% FBS, to explore NPs behaviour in presence of serum proteins.

H₂O: As shown in Figure 21, Dim₅_IR780@HSA displayed an excellent stability in aqueous solution and a good colloidal stability, showing an average diameter of about 130 nm and PDI of 0.1 over 96 h.

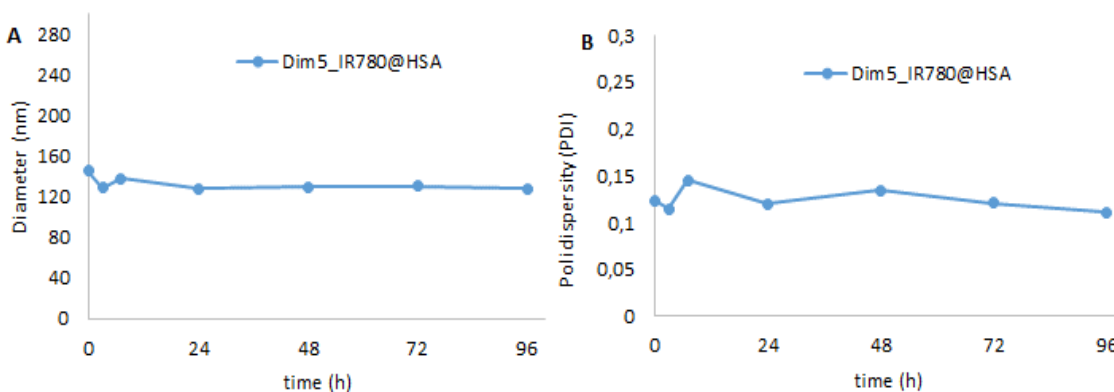


Figure 21 Stability of Dim₅_IR780@HSA in H₂O. (A) Diameter. (B) PDI

PBS: Figure 22 indicated the significant stability of Dim₅_IR780@HSA also in saline solution at 37°C, over 96 h, showing an average diameter of about 130 nm and PDI ranging between 0.13 to 0.16.

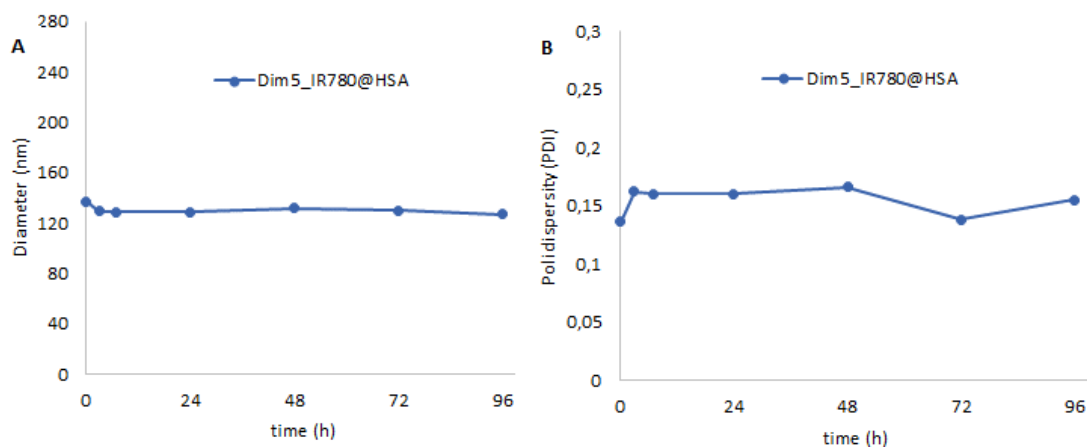


Figure 22 Stability of Dim₅_IR780@HSA in PBS. (A) Diameter. (B) PDI

PBS with 10% FBS at pH=7.4: Under these conditions, in the first 48 hours, we observed a gradual increase in NPs size up to 160 nm, probably due to the corona effect of FBS protein (Figure 23A). Conversely, the PDI values (around 0.25) were quite stable over the time (Figure 23B).

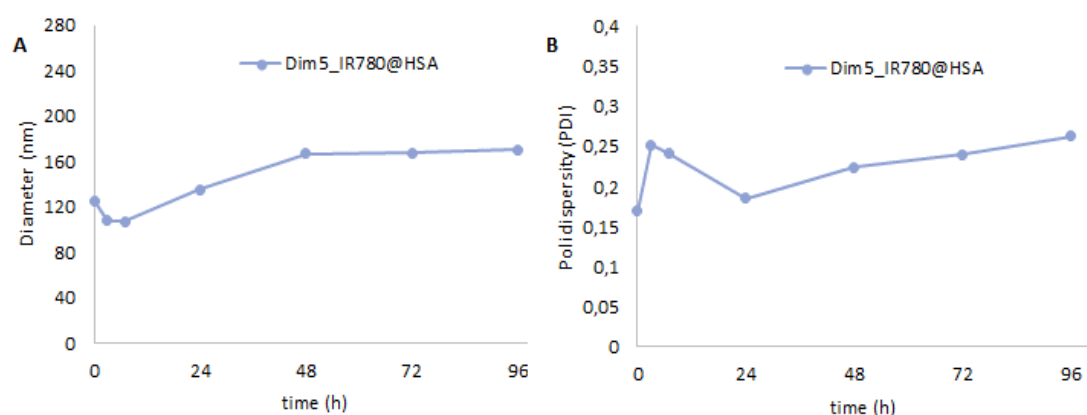


Figure 23 Stability of Dim₅_IR780@HSA (blue line) in PBS+ FBS 10%. (A) Diameter. (B) PDI

3.3.3 Stability of Dim₁₂@NPs

The stability of Dim₁₂@NPs was evaluated at 37°C by performing DLS analysis at different time intervals (0, 3, 24, 72, 144 and 168 h) and under five different conditions:

- H₂O;
- PBS at pH = 7.4;
- PBS + 10% FBS, to explore NPs behaviour in presence of serum proteins;
- BSA (bovine serum albumin, 35 mg/mL) in H₂O, to evaluate whether tEB moiety could efficiently bind to HSA *in vivo*;
- BSA (35 mg/mL) in PBS.

H₂O: As shown in Figure 24, Dim₁₂@NPs demonstrated an excellent stability in aqueous solution, with an average hydrodynamic diameter around 80 nm and PDI around 0.25.

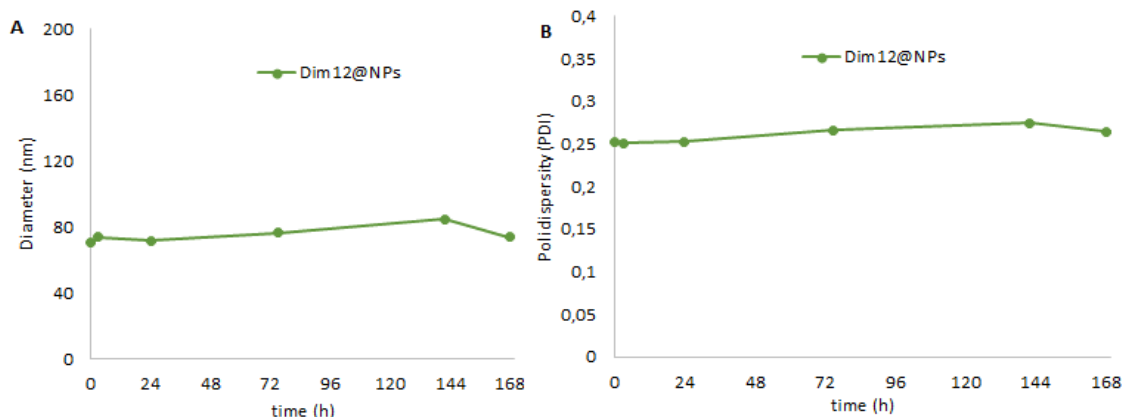


Figure 24 Stability of Dim₁₂@NPs in H₂O. (A) Diameter. (B) PDI.

PBS at pH=7.4: Nanoparticles revealed a good stability also in saline solution, showing an average diameter ranging between 70 and 90 nm and PDI of about 0.25 (Figure 25A and B).

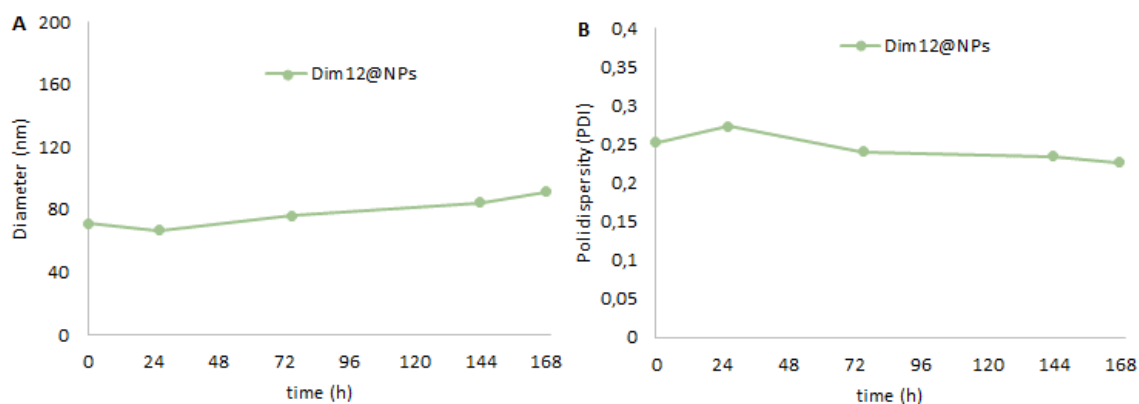


Figure 25 Stability of Dim₁₂@NPs in PBS at pH=7.4. (A) Diameter. (B) PDI.

PBS + 10% FBS: Under these conditions, we observed a considerable increase up to 1000 nm, accompanied by the appearance of a white precipitate, probably due to an aggregation process.

BSA in H₂O and PBS:⁴⁴ Dim₁₂@NPs demonstrated an excellent stability in presence of BSA both in aqueous and saline solutions. Indeed, in H₂O, NPs displayed an average size around 80 nm and a PDI ranging between 0.15 to 0.3 (Figure 26), while, in PBS, nanoparticles are smaller and show an excellent diameter of 25 nm and PDI around 0.3 (Figure 11). It is worth noting that these data confirmed the capability of Dim₁₂@NPs of binding albumin, thanks to the

presence of tEB moiety, leading to the formation of stable nanocomplexes.⁴⁴

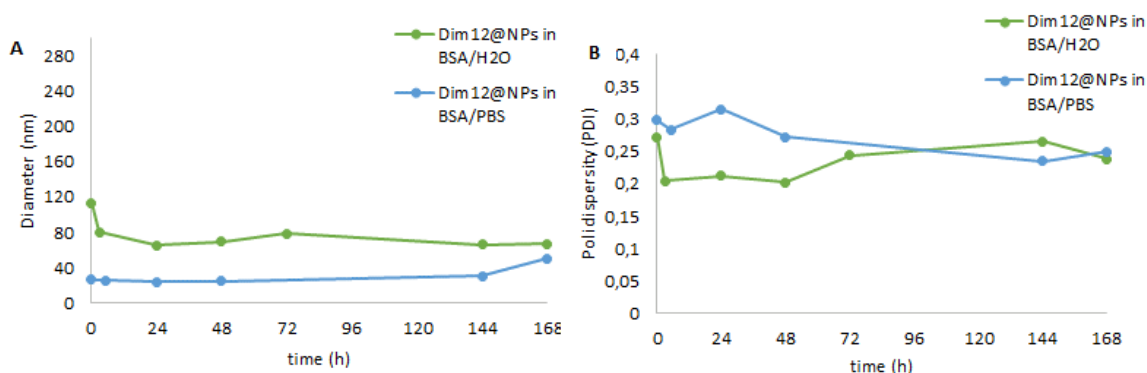


Figure 26 Stability of Dim12@NPs in BSA in H₂O (green line) and in PBS (blue line). (A) Diameter. (B) PDI.

3.4. Reactive oxygen species production

IR780 dye is a photosensitizer that, upon NIR light activation, can generate radicals, acting as cytotoxic agents. Therefore, we evaluated the ability of Dim₅_IR780@HSA to produce ROS, by using the chemical probe 2,7-dichlorofluorescein diacetate (DCF-DA).

In this method, the non-fluorescent molecule DCF-DA is initially hydrolysed by NaOH solution (0.01 M), into 2,7-dichlorodihydrofluorescein (DCFH₂). Upon oxidation by ROS and ¹O₂, the non-fluorescent DCFH₂ is converted to the highly fluorescent 2,7-dichlorofluorescein (DCF), which can be detected through its absorption band at 500 nm (Figure 27).

The intensity of the DCF absorption band is correlated to the quantity of generated ROS.⁵⁵

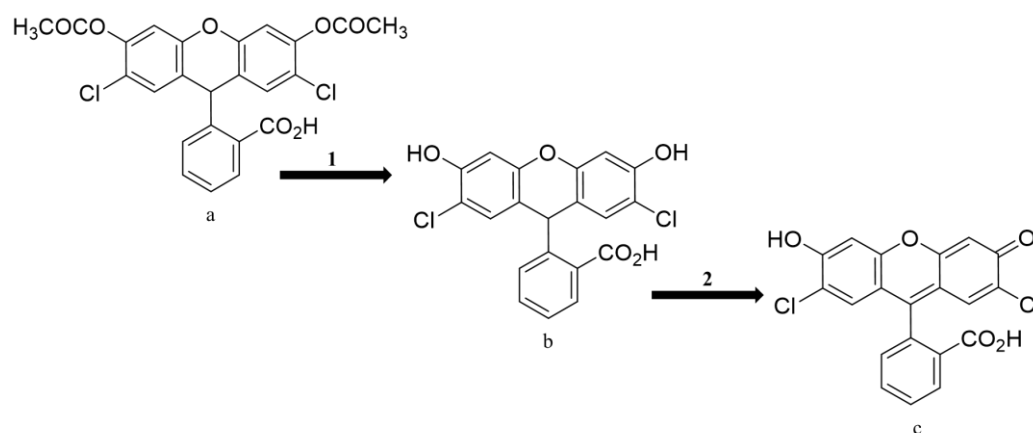


Figure 27 Oxidation mechanism of DCF-DA. In the first step (1), DCF-DA (a) is hydrolysed in DCFH₂ (b) by a NaOH solution 0.01 M; in second step (2) DCFH₂ is oxidated in DCF (c) by ROS.

For this experiment, a solution of Dim₅_IR780@HSA and ROS probe (see experimental procedure in section 5.5) was irradiated with a tungsten lamp and, as shown in Figure 28, the DCF absorption at 500 nm increased proportionally

with increasing the irradiation time.

Thus, even when loaded into NPs and in the presence of Dim₅, IR780 efficiently produces ROS in a light dose-dependent manner. It is worth noticing that at t=0, no ROS production was observed, confirming that IR780 released ROS only upon light irradiation, thus make this nanosystem suitable for controlled ROS-triggered PTX release.

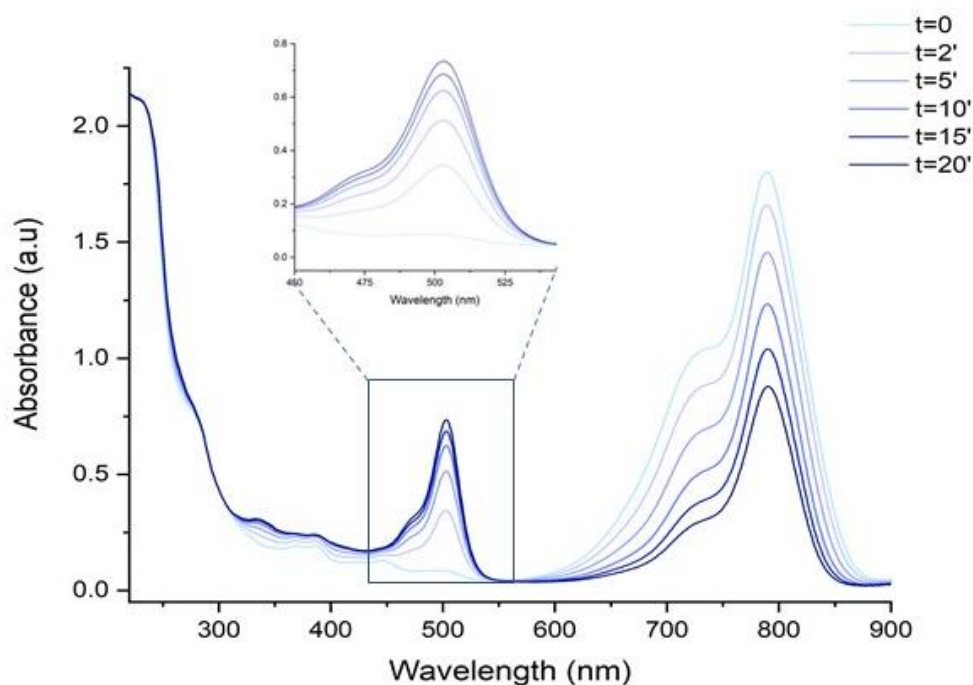


Figure 28 Dim₅_IR780@HSA ROS production

3.5 *In vitro* drug release profiles

As bioresponsive prodrugs, the herein synthesized dimers are expected to be hydrolysed under the specific redox conditions within tumor, improving their selectivity and effectiveness.⁵⁶ In this regard, we next assessed the ability of Dim₅@HSA to release PTX in oxidative environment.

To investigate dimers release kinetics, 0.6 mL of an aqueous solution of Dim₅@HSA and Dim₅_IR780@HSA (2 mg/mL), were inserted in a dialysis bag (cut-off 14 kDa), at 37°C against:

- (i) PBS/EtOH (10 mL; 10% EtOH) solution pH 7.4 in the dark;
- (ii) oxidative conditions: H₂O₂ (10 mM) in PBS/EtOH (10 mL; 10% EtOH) solution at pH 7.4, in the dark;
- (iii) PBS/EtOH (10 mL; 10% EtOH) solution pH 7.4, under light irradiation;
- (iv) oxidative conditions: H₂O₂ (10 mM) in PBS/EtOH (10 mL; 10% EtOH) solution

at pH 7.4, under light irradiation.

At selected time points, 200 μ L of each sample were withdrawn and replenished with fresh medium up to 5 h, and then analysed by HPLC (detection UV-DAD, 200-800 nm). HPLC analysis was performed using the gradient mobile phase shown in Figure 29 (H₂O + TFA 0.1% v / v) / (ACN + TFA 0.1% v / v), which allowed to identify the following retention times:

PTX (t_R=5,7 min, 228 nm).

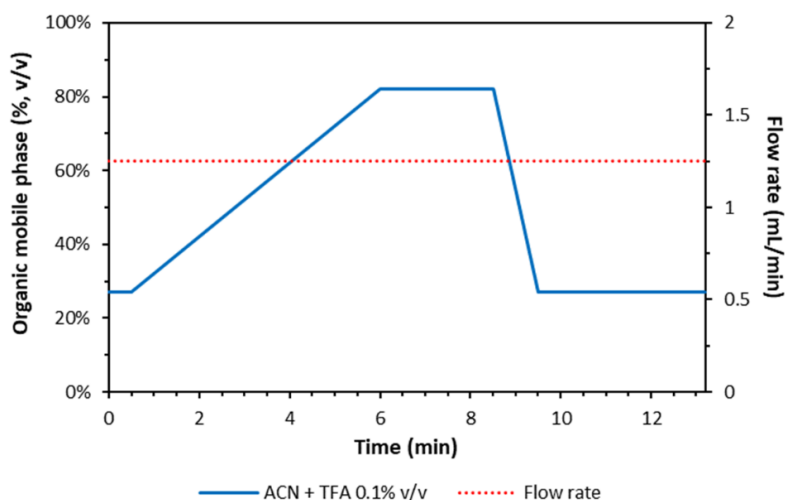


Figure 29 HPLC gradient for release kinetics analysis

DARK, Figure 30 A: in the presence of 10 mM H₂O₂, the percentage of released PTX reached about 2.5 % in Dim₅@HSA (cyan line) and 2% in Dim₅_IR780@HSA (yellow line), while in PBS dimer **5** displayed the slowest drug release in both nanoformulations.

LIGHT, Figure 30 B: as indicated by yellow and orange lines, Dim₅_IR780@HSA slight increase the percentage of free PTX, reaching about 3%. Conversely, in Dim₅@HSA, we did not appreciate any significant increase in drug release.

Based on the above results, we could speculate that upon light activation, IR780 produce ROS, triggering the faster PTX release from nanoparticles. However, owing to the harsh release conditions required for PTX release from **5**, and to improve the controlled PTX release kinetics, we are going to prepare and investigate further dimers, bearing different linkers.

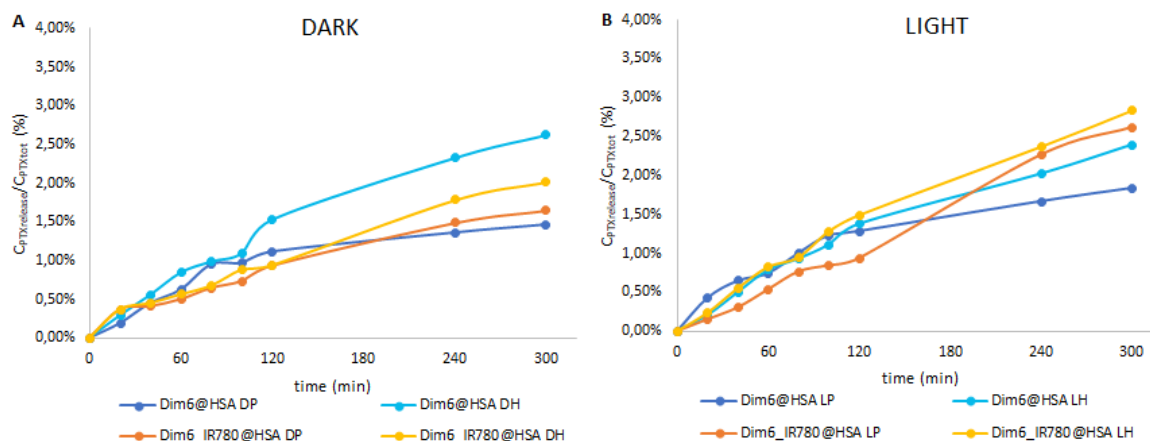


Figure 30 (A) **5** degradation at the dark and (B) **5** degradation at the light from Dim₅@HSA and Dim₅_IR780@HSA at pH 7,4. D= at the dark, L= at the light, H= in 10 mM H₂O₂, P=in PBS/EtOH

Based on the HPLC results and on the literature, the H₂O₂-triggered degradation mechanism of dimer **5** is depicted in Figure 31.⁴⁷

Firstly, thioketal linker is slowly cleaved into two sulfydyl, followed by the oxidation of the sulfydyl to hydrophilic sulfoacid, leading to release of active PTX molecules.

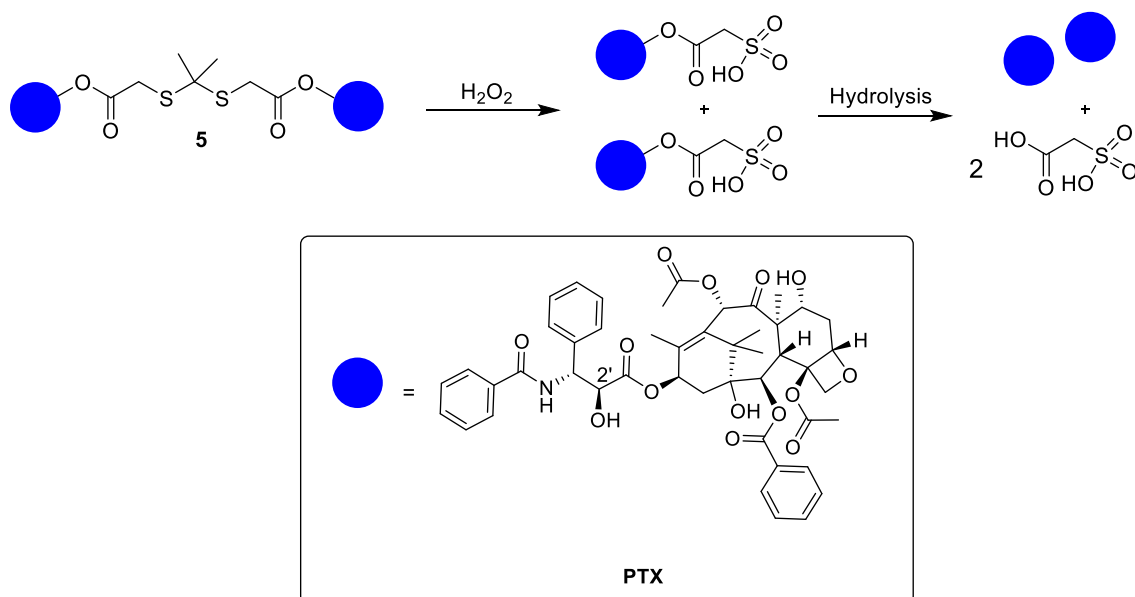


Figure 31 The proposed degradation mechanism of dimer **5** in presence of H₂O₂

4. CONCLUSIONS

In this thesis work, five dimeric prodrugs of PTX, **4**, **5**, **6**, **8** and **12**, were synthesized and characterized through NMR spectroscopy. Remarkably, compounds **5** and **12** are herein described for the first time, and it worth evidencing that **12** contains a truncated Evans Blue (tEB) moiety, that exhibits selective and reversible binding to HSA.

Indeed, in the second part of the project, the research group and I envisioned the possibility to self-assemble these compounds into stable nanoparticles. To increase the anticancer efficacy of the obtained nanosystems, I further encapsulated a photosensitizer, e.g., IR780, within nanoparticles, aimed at (i) exploiting the synergism between chemo- and photodynamic therapy, and (ii) at promoting, upon light activation, the ROS-triggered release of PTX.

In details, I prepared two different nanoformulations:

- HSA-based nanoparticles, Dim₅_IR780@HSA and Dim₅@HSA;
- PTX dimer-based nanoparticles, Dim₁₂@NPs, capable of *in vivo* binding endogenous HSA, thanks to the presence of tEB moiety.

Dynamic Light Scattering (DLS) analyses showed that Dim₅@HSA and Dim₅_IR780@HSA displayed an excellent hydrodynamic diameter ranging from 110 to 150 nm, and a good PDI (around 0.15). UV-Vis spectroscopy study on Dim₅_IR780@HSA accounted for the effective IR780 loading, as well as for their ability to efficiently produce ROS in a light dependent manner. Furthermore, release studies were conducted on Dim₅@HSA and Dim₅_IR780@HSA in the presence of PBS or H₂O₂ in the dark or light. Our results indicate that PTX release is strictly influenced by both the presence of H₂O₂ and IR780, thus Dim₅_IR780@HSA showed a slightly faster PTX release upon light irradiation and in oxidative conditions. On the other hand, Dim₁₂@NPs showed an optimal average diameter below 80 nm and a good PDI (0.25).

Finally, to evaluate whether tEB moiety could efficiently bind to HSA *in vivo*, DLS analysis was performed on Dim₁₂@NPs after their incubation with a BSA solution for different time intervals. Our results showed a significant decrease of nanoparticles' size (up to 20-30 nm) upon the exposure to BSA, confirming the effective formation of small prodrug/albumin nanoaggregates.

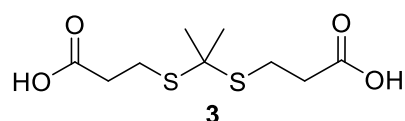
All obtained nanoparticles exhibited an extraordinary colloidal stability in water and in a physiological environment.

At present, experiments are ongoing on derivatives **5** and **12** to further characterise compounds by LC-MS. As concerning nanoparticles, further studies are ongoing in terms of morphology and drug release profiles.

Future perspectives of this work include the encapsulation of IR780 within Dim₁₂@NPs, following by all characterization studies (DLS, stability, drug release kinetics). Once optimized, the nanosystems will be evaluated for their in vitro anticancer activity.

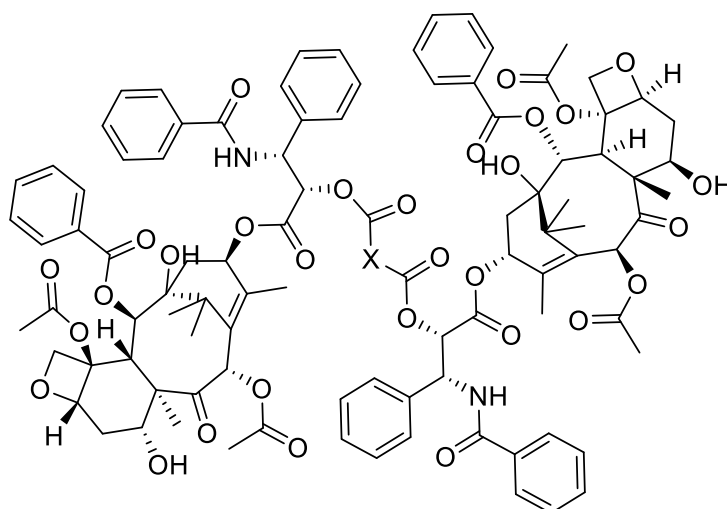
temperature for 5 h. The mixture was then placed in ice bath, filtered and washed with hexane and water 3 times to obtain the white product with a yield of 26%. $^1\text{H NMR}$ (400 MHz, CD_3OD): δ 1.04 (s, 6H), 2.86 (s, 4H).

Synthesis of compound 3



TFA (50 μL) was added dropwise to a solution of 3-mercaptopropanoic acid (1.64 mL, 18.8 mmol, 1 eq) dissolved in 3.5 mL of anhydrous acetone and stirred at room temperature for 7 h. Et_2O (3mL) was added at the solution and the mixture was then placed in ice bath, filtered and washed with hexane 2 times to obtain the white product with a yield of 31%. $^1\text{H NMR}$ (400 MHz, CDCl_3) δ 2.91 (t, $J = 7.4$ Hz, 4H), 2.68 (t, $J = 7.5$ Hz, 4H), 1.60 (s, 6H).

Synthesis of compounds 4-6



4: X = $-\text{CH}_2-\text{S}-\text{CH}_2-$;

5: X = $-\text{CH}_2-\text{S}-\text{C}(\text{CH}_3)_2-\text{S}-\text{CH}_2-$;

6: X = $\text{CH}_2-\text{CH}_2-\text{S}-\text{C}(\text{CH}_3)_2-\text{S}-\text{CH}_2-\text{CH}_2-$;

PTX (150 mg, 0.1757 mmol, 2.2 eq) was dissolved in anhydrous CH_2Cl_2 (2 mL) followed by sequential addition of dicarboxylic acid (0.080 mmol, 1 eq), EDC \cdot HCl (0.383 mmol, 4.8 eq) and DMAP (0.024 mmol, 0.3 eq) under argon atmosphere. After 1h, further 0.185 mmol of EDC \cdot HCl and 0.024 mmol of DMAP were added

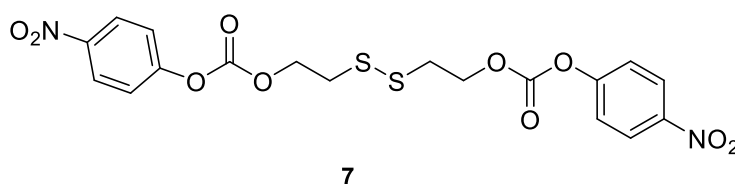
to the reaction mixture. The mixture was stirred for 24h at room temperature and the progress of the reaction was monitored by TLC (cyclohexane/ethyl acetate 2:1). The organic layers were washed with 0.1 N HCl (2 time), dried over Na₂SO₄ and concentrated under reduced pressure. The crude product was purified by silica gel column chromatography using cyclohexane/ethyl acetate (1:1 v/v) as the eluent.

4: white solid. Y = 40%; ¹H NMR (500 MHz, CDCl₃) δ 8.16 (d, *J* = 7.4 Hz, 4H), 7.74 (d, *J* = 7.6 Hz, 4H), 7.66–7.58 (m, 2H), 7.56–7.49 (m, 4 H), 7.48–7.31 (m, 16 H), 7.26–7.21 (m, NH, 2 H), 6.34–6.19 (m, 4 H), 6.09 (dd, *J* = 9.3, 2.5 Hz, 2 H), 5.68 (d, *J* = 7.1 Hz, 2 H), 5.53 (d, *J* = 2.9 Hz, 2 H), 4.98 (d, *J* = 8.6 Hz, 2 H), 4.43 (dd, *J* = 10.8, 6.7 Hz, 2 H), 4.32 (d, *J* = 8.4 Hz, 2 H), 4.21 (d, *J* = 8.4 Hz, 2 H), 3.81 (d, *J* = 7.0 Hz, 2 H), 3.27 (d, *J* = 14.7. Hz, 2 H), 3.16 (d, *J* = 14.7. Hz, 2 H), 2.63–2.52 (m, 2 H), 2.49 (s, 6 H), 2.39 (dd, *J* = 15.3, 9.4 Hz, 2 H), 2.22 (s, 6 H), 2.19–2.12 (m, 2 H), 1.89 (s, 6 H), 1.69 (s, 6 H), 1.22 (s, 6 H), 1.14 (s, 6 H).

5: white solid. Y = 71%; ¹H NMR (400 MHz, CDCl₃) δ 8.17-8.10 (m, 2H), 7.74 (d, *J* = 7.3 Hz, 2H), 7.62 (t, *J* = 7.4 Hz, 1H), 7.54-7.32 (m, 10H), 7.01 (d, *J* = 9.1 Hz, 1H), 6.31-6.19 (m, 2H), 5.97 (dd, *J* = 9.2, 3.3 Hz, 1H), 5.68 (d, *J* = 7.1 Hz, 1H), 5.53 (t, *J* = 4.9 Hz, 1H), 4.97 (d, *J* = 7.7 Hz, 1H), 4.44 (dd, *J* = 10.9, 6.6 Hz, 1H), 4.32 (d, *J* = 8.4 Hz, 1H), 4.20 (d, *J* = 8.4 Hz, 1H), 3.80 (d, *J* = 7.1 Hz, 1H), 2.85-2.63 (m, 4H), 2.61-2.50 (m, 1H), 2.46 (d, *J* = 5.8 Hz, 3H), 2.40- 2.28 (m, 1H), 2.25-2.20 (m, 3H), 2.18-2.08 (m, 1H), 1.97-1.83 (m, 4H), 1.68 (s, 3H), 1.58 (s, 3H), 1.24-1.19 (m, 3H), 1.13 (s, 3H). M

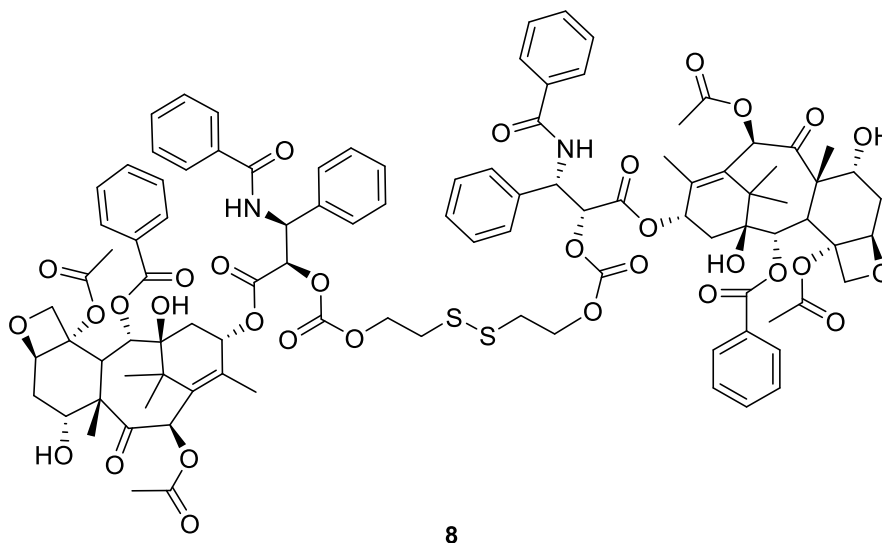
6: white solid. Y = 82%; ¹H NMR (400 MHz, CDCl₃) δ 8.17-8.10 (m, 2H), 7.74 (d, *J* = 7.3 Hz, 2H), 7.62 (t, *J* = 7.4 Hz, 1H), 7.54-7.32 (m, 10H), 7.01 (d, *J* = 9.1 Hz, 1H), 6.31-6.19 (m, 2H), 5.97 (dd, *J* = 9.2, 3.3 Hz, 1H), 5.68 (d, *J* = 7.1 Hz, 1H), 5.53 (t, *J* = 4.9 Hz, 1H), 4.97 (d, *J* = 7.7 Hz, 1H), 4.44 (dd, *J* = 10.9, 6.6 Hz, 1H), 4.32 (d, *J* = 8.4 Hz, 1H), 4.20 (d, *J* = 8.4 Hz, 1H), 3.80 (d, *J* = 7.1 Hz, 1H), 3.42 (d, *J* = 2.9 Hz, 2H), 2.54 (ddd, *J* = 15.9, 9.6, 6.6 Hz, 1H), 2.44 (d, *J* = 7.8 Hz, 2H), 2.39 – 2.27 (m, 1H), 2.26 – 2.19 (m, 2H), 2.12 (dd, *J* = 15.4, 8.9 Hz, 1H), 1.97-1.83 (m, 4H), 1.68 (s, 3H), 1.58 (s, 3H), 1.24-1.19 (m, 3H), 1.13 (s, 3H).

Synthesis of compound 7



To a solution of bis-(2-hydroxyethyl)disulfide (1.08 g, 7.00 mmol, 1 eq) in DCM (8 mL) *p*-nitrophenylchloroformate (21 mmol, 3 eq) and *N,N*-diisopropylethylamine (DIPEA) (17.5 mmol, 2.5 eq) were added under nitrogen atmosphere. The mixture was stirred at room temperature for 4 h. The progress of the reaction was monitored by thin layer chromatography (TLC) using ethyl acetate: hexane (2:4). The organic layers were washed with HCl 1N and saturated NaHCO₃, dried over Na₂SO₄, filtered, and concentrated under reduced pressure. The crude was purified by silica gel column chromatography using cyclohexane/ethyl acetate (4:2 v/v) as the eluent. A white solid was obtained (Y= >98%). ¹H NMR (400 MHz; CDCl₃): δ 8.28 (d, *J* = 9.2 Hz, 4H), 7.39 (d, *J* = 9.2 Hz, 4H), 4.57 (t, *J* = 6.5 Hz, 4H), 3.08 (t, *J* = 6.4 Hz, 4H).

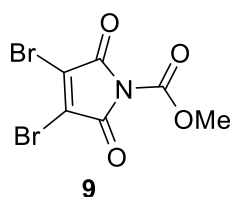
Synthesis of compound 8



To a solution of compound 7 (38.4 mg, 0.084 mmol) in DCM (1.53 mL), paclitaxel (150 mg, 0.176 mmol) and a catalytic amount of DMAP (22.4 mg, 0.183 mmol) were added under nitrogen atmosphere overnight. The progress of the reaction was monitored by thin layer chromatography (TLC) using ethyl acetate: hexane (1:1). The reaction mixture was washed with HCl 0.1N, saturated NaHCO₃ and brine, then, dried over Na₂SO₄, filtered, concentrated and purified by flash column chromatography using cyclohexane/ethyl acetate (1:1 v/v) as the eluent. The

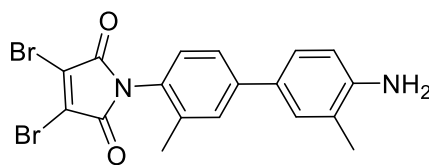
product was obtained in 83% yield as a white solid. $^1\text{H NMR}$ (400 MHz, CDCl_3) δ 8.14 (d, $J = 7.1$ Hz, 4H), 7.72 (d, $J = 7.1$ Hz, 4H), 7.60 (d, $J = 7.6$ Hz, 2H), 7.55 – 7.32 (m, 10H), 6.96 (d, $J = 9.4$ Hz, 1H), 6.29 (s, 1H), 6.26 (dd, $J = 9.2, 1.7$ Hz, 1H), 6.00 (dd, $J = 9.4, 2.9$ Hz, 2H), 5.68 (d, $J = 7.0$ Hz, 1H), 5.44 (d, $J = 2.9$ Hz, 2H), 4.97 (dd, $J = 9.8, 2.5$ Hz, 2H), 4.47 – 4.28 (m, 5H), 4.20 (dd, $J = 8.4, 0.7$ Hz, 2H), 3.81 (d, $J = 7.0$ Hz, 2H), 2.88 (t, $J = 6.5$ Hz, 1H), 2.49 (d, $J = 4.1$ Hz, 2H), 2.46 (s, 5H), 2.41 – 2.35 (m, 1H), 2.21 (s, 8H), 2.17 (s, 1H), 1.92 (d, $J = 1.3$ Hz, 5H), 1.76 (s, 2H), 1.68 (s, 4H), 1.61 (s, 9H), 1.27 (s, 3H), 1.23 (s, 5H), 1.13 (s, 3H)

Synthesis of compound 9



To a solution of 3,4-dibromo-1H-pyrrole-2,5-dione (800 mg, 3.14 mmol, 1 eq) in 25 mL of anhydrous THF, were added *N*-methylmorpholine (345 μL , 3.14 mmol, 1 eq) and methyl chloroformate (243 μL , 3.14 mmol, 1 eq) at room temperature, under nitrogen atmosphere. The mixture was stirred for 1 h, afterwards 30 mL of CH_2Cl_2 were added to the reaction and then the combined organic phases were washed with H_2O and brine, dried over Na_2SO_4 , filtered, and concentrated *in vacuo*. The compound was obtained in 80% yield as a purple solid. $^1\text{H NMR}$ (400 MHz, CDCl_3) δ 4.00 (s, 3H).

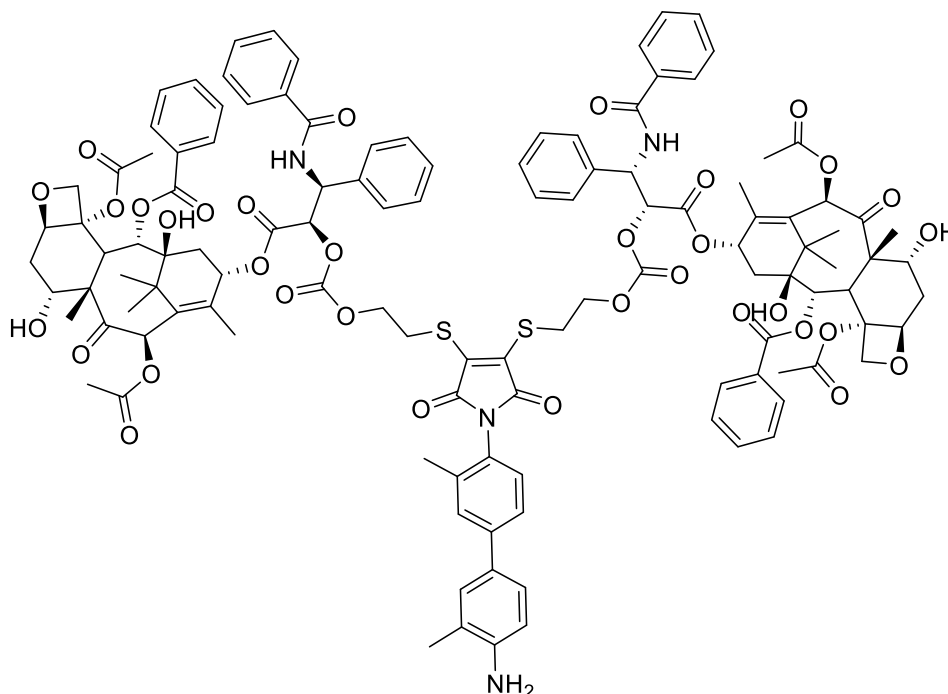
Synthesis of compound 10



To a solution of compound **9** (200 mg, 0.639 mmol, 1 eq) in 24 mL of anhydrous DCM, *o*-tolidine (163 mg, 0.767 mmol, 1.2 eq) was added at room temperature, under nitrogen atmosphere. The mixture was stirred for 19 h and the progress of the reaction was monitored by thin layer chromatography (TLC) using ethyl acetate: hexane (2:3). Solvent was removed under reduced pressure. The crude was purified by silica gel column chromatography using cyclohexane/ethyl acetate

(3:2) as the eluent. The product was obtained in 27% yield as a yellow solid. ^1H NMR (400 MHz, CDCl_3) δ 7.47 (s, 1H), 7.44 (dd, $J = 8.2, 2.0$ Hz, 1H), 7.31 – 7.26 (m, 2H), 7.12 (d, $J = 8.1$ Hz, 1H), 6.74 (d, $J = 8.0$ Hz, 1H), 2.24 (dd, $J = 13.9, 7.5$ Hz, 6H).

Synthesis of compound 11

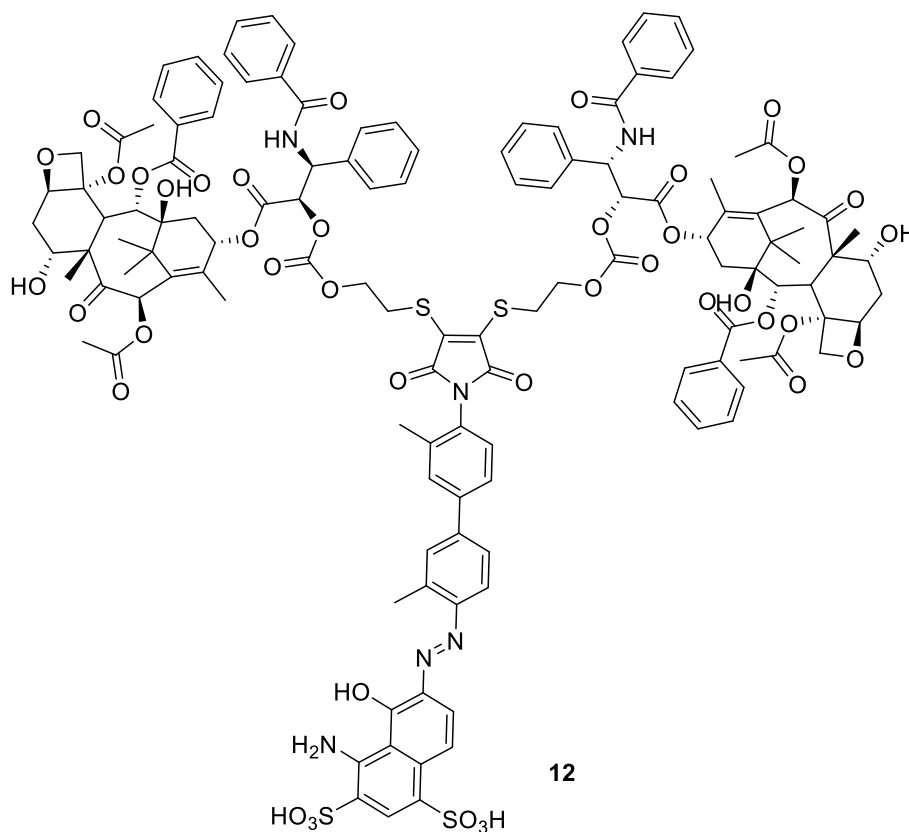


11

Compound **8** (80 mg, 0,042 mmol, 1 eq) was dissolved in anhydrous THF (1.25 mL) followed by the addition of compound **10** (22.5 mg, 0,050 mmol, 1,2 eq) dissolved in 3,75 mL of MeOH, TCEP (30 mg, 0.104 mmol, 2.5 eq) and DIPEA (43.8 μL , 0.251 mmol, 6 eq) under argon atmosphere. The yellow reaction mixture was stirred for 2 h at room temperature and the progress of the reaction was monitored by TLC (ethyl acetate/cyclohexane/methanol 9:6:0.25). The mixture was washed with 0.1 N HCl and brine, dried over Na_2SO_4 and concentrated under reduced pressure. The crude material was then purified on a silica gel flash column chromatography (eluent: ethyl acetate/cyclohexane/methanol 9:6:0.25) to obtain compound **11** as a yellow solid (Y=83%). ^1H NMR (400 MHz, CDCl_3) δ 8.16 (d, $J = 13.5, 8.2$ Hz, 2H), 7.71 (dd, $J = 7.8, 5.3, 4.4$ Hz, 2H), 7.63 – 7.55 (m, $J = 10.5, 4.3$ Hz, 1H), 7.49 (t, 4H), 7.45 – 7.28 (m, 10H), 7.05 (d, $J = 7.3$ Hz, 1H), 6.97 (t, 1H), 6.72 (d, 1H), 6.33 – 6.19 (m, 2H), 5.98 (d, $J = 10.5$ Hz, 1H), 5.68 (d, 1H), 5.46 – 5.41 (m, 1H), 4.96 (d, $J = 9.3$ Hz, 1H), 4.51 – 4.26 (m, 2H), 4.21 (d, $J = 10.3$ Hz,

1H), 3.82 (d, $J = 16.0, 7.3$ Hz, 1H), 3.63 – 3.48 (m, 2H), 2.64 – 2.30 (m, 7H), 2.29 – 2.10 (m, 4H), 2.01 – 1.54 (m, 10H), 1.37 – 1.19 (m, 3H), 1.11 (s, 3H).

Synthesis of compound 12



Compound 11 (25 mg, 0.0114 mmol, 1 eq) was dissolved in acetonitrile (0.116 mL) in a glass vial and cooled at 0°C, then HCl (0.3 M, 0.116 mL) was added. 0.039 mL of cold aqueous sodium nitrite solution (2.4 mg, 0.034 mmol, 3 eq) was dropped and the reaction mixture was stirred for 20 min, the reaction mixture turned orange, confirming the formation of diazonium salt. This solution was added dropwise under vigorous stirring to a cold solution of 1-amino-8-naphtol-2,4-disulfonic acid monosodium salt (4.3 mg, 0.0125 mmol, 1.1 eq), $NaHCO_3$ (3.4 mg, 0.041 mmol, 3.6 eq) in water (0.135 mL) at 0 °C. The solution turned violet. The mixture was further stirred for 3 hours at 10°C.

Then the mixture was concentrated and the solid was dissolved in 1 mL of water/methanol (1:5) and purified through dialysis bag (MWCO: 12 kDa) against milliQ H_2O /ethanol 80:20 first, then with only H_2O (x4) during 24 h. After purification, the solution was lyophilized in the dark, obtaining a purple solid 12 (Y= 50 %). 1H NMR (400 MHz, d_6 -DMSO) δ 9.32 (d, $J = 17.2$ Hz, 1H), 7.97 (d, $J = 7.8$

Hz, 1H), 7.84 (d, $J = 6.4$ Hz, 1H), 7.71 (ddd, $J = 7.8, 5.3, 4.4$ Hz, 4H), 7.63 – 7.55 (m, $J = 10.5, 4.3$ Hz, 2H), 7.49 (t, 6H), 7.45 – 7.28 (m, 16H), 7.05 (d, $J = 7.3$ Hz, 1H), 6.97 (t, 2H), 6.72 (d, 1H), 6.33 – 6.19 (m, 2H), 5.98 (d, $J = 10.5$ Hz, 1H), 5.68 (d, 1H), 5.46 – 5.41 (m, 1H), 4.96 (d, $J = 9.3$ Hz, 1H), 4.51 – 4.26 (m, 6H), 4.21 (d, $J = 10.3$ Hz, 2H), 3.82 (d, $J = 16.0, 7.3$ Hz, 2H), 3.63 – 3.48 (m, 2H), 2.64 – 2.30 (m, 14H), 2.29 – 2.10 (m, 14H), 2.01 – 1.54 (m, 26H), 1.37 – 1.19 (m, 14H), 1.11 (s, 6H).

5.2 Preparation of nanoparticles

Preparation of Dim₅@HSA

HSA was dissolved in 2.8 mL of milliQ H₂O (3.7 mg/mL) and 185 μ L of ethanolic mixture of 18% w/w_{HSA} of dimer **5** (10 mg/mL) was slowly added into solution under vigorous stirring. After 10 minutes, dimensions were monitored by DLS: $d = 123$ nm and PDI = 0.115.

Preparation of Dim₅ IR780@HSA

HSA was dissolved in 2.8 mL of H₂O (3.7 mg/mL) and 185 μ L of ethanolic mixture of 18% w/w_{HSA} of dimer **5** (10 mg/mL) and 7% w/w_{HSA} of IR780 (8 mg/mL), was slowly added into solution under vigorous stirring. After 10 minutes, dimensions were monitored by DLS: $d = 136$ nm and PDI = 0.157.

Preparation of Dim₁₂@NPs

A solution of 66 μ L of dimer **12** (15 mg/mL) in DMSO was slowly added into 0.93 mL H₂O or PBS (1 mg/mL), under vigorous stirring. After 10 minutes, dimensions were monitored by DLS: in H₂O $d = 71.0$ nm and PDI = 0.252; in PBS $d = 175$ nm and PDI = 0.263.

5.3 Stability of NPs

Stability of Dim₅@HSA and Dim₅ IR780@HSA

To investigate colloidal stability, 0.2 mL of NPs solution were added in 1.6 mL solution of (i) H₂O, (ii) PBS, and (iii) PBS with 10% FBS. The samples were incubated at temperature of 37 °C and changes in hydrodynamic diameter and PDI were monitored by DLS at different time intervals (0, 3, 7, 24, 48, 72 and 96 h).

Stability of Dim₁₂@NPs

To investigate colloidal stability, NPs solution were added in 1.6 mL solution of (i) H₂O, (ii) PBS, (iii) PBS with 10% FBS, (iv) BSA (35 mg/mL) in H₂O, and (v) BSA (35 mg/mL) PBS. Samples were incubated at 37°C, and changes in hydrodynamic diameter and PDI were monitored by DLS at different time intervals (0, 3, 24, 72, 144 and 168 h).

5.4. *In vitro* drug release profile

To evaluate the drug release profile, Dim₅@HSA and Dim₅_IR780@HSA were analysed in 4 different conditions:

- (1) PBS with 10% EtOH solution, dark;
- (2) H₂O₂ (10 mM) in PBS/EtOH, (9/1), dark;
- (3) PBS with 10% EtOH solution, light;
- (4) H₂O₂ (10 mM) in PBS/EtOH, (9/1), light.

In details, Dim₅@HSA was dissolved in 3 mL of H₂O, then 0.6 mL of NPs solution were inserted in dialysis bag (MWCO: 14 kDa) (4 samples). According to the above-described protocol, also Dim₅_IR780@HSA was put into dialysis bag (4 samples).

Then, the eight dialysis bags have been placed in eight different vials containing 10 mL of different solutions (1-4) and incubated at 37°C. At selected time points (20', 40', 1h, 1h 20', 1h 40', 2h, 4h, 5h) 200 µL of each sample were withdrawn and replenished with fresh solution up to 6h. All of samples drawn were analysed by HPLC (detection UV-DAD, 200-800 nm), using the gradient mobile phase (H₂O + TFA 0.1% v / v) / (ACN + TFA 0.1% v / v), which allowed to identify PTX (t_R=5,7 min, 228 nm).

5.5. Reactive oxygen species production

ROS generation was determined for Dim₅_IR780@HSA, by using the chemical probe 2,7-dichlorofluorescein diacetate (DCF-DA). Briefly, 2 mL of NaOH (0.01 M) were added to 500 µL of DCF-DA in methanol solution (0.54 mg/mL) and stirred, in the darkness, for 30 min at room temperature; afterward 10 mL of PBS at 7.4 pH were added providing the ROS probe solution. Subsequently, 100 µL of Dim₅_IR780@HSA were added to a cuvette containing 182 µL of milliQ H₂O, 500 µL of PBS (pH 7.4), and 218 µL of ROS probe as previously prepared. The solution was irradiated with tungsten lamp (Philips; 300 W) at a distance of 30 cm for 2, 5,

10, 15 and 30 min and the absorbance spectra were recorded at each time point with a UV-Vis spectrophotometer, reading the DCF peak increase at 500 nm.

6. BIBLIOGRAPHY

1. Sung, H. *et al.* Global Cancer Statistics 2020: GLOBOCAN Estimates of Incidence and Mortality Worldwide for 36 Cancers in 185 Countries. *CA. Cancer J. Clin.* **71**, 209–249 (2021).
2. Mohla, S. Tumor microenvironment. *J. Cell. Biochem.* **101**, 801–804 (2007).
3. Zhang, Y. & Zhang, Z. The history and advances in cancer immunotherapy: understanding the characteristics of tumor-infiltrating immune cells and their therapeutic implications. *Cell. Mol. Immunol.* **17**, 807–821 (2020).
4. Weber, C. E. & Kuo, P. C. The tumor microenvironment. *Surg. Oncol.* **21**, 172–177 (2012).
5. Nallanthighal, S., Heiserman, J. P. & Cheon, D.-J. The Role of the Extracellular Matrix in Cancer Stemness. *Front. Cell Dev. Biol.* **7**, 1–14 (2019).
6. Ralph, S. J., Nozuhur, S., Moreno-Sanchez, R., Enriquez, S. R. & Pritchard, R. NSAID celecoxib: a potent mitochondrial pro-oxidant cytotoxic agent sensitizing metastatic cancers and cancer stem cells to chemotherapy. *J. Cancer Metastasis Treat.* **4**, 49 (2018).
7. Barar, J. & Omid, Y. Dysregulated pH in tumor microenvironment checkmates cancer therapy. *BiolImpacts* **3**, 149–162 (2013).
8. Such, G. K., Yan, Y., Johnston, A. P. R., Gunawan, S. T. & Caruso, F. Interfacing Materials Science and Biology for Drug Carrier Design. *Adv. Mater.* **27**, 2278–2297 (2015).
9. Yang, B., Chen, Y. & Shi, J. Reactive Oxygen Species (ROS)-Based Nanomedicine. *Chem. Rev.* **119**, 4881–4985 (2019).
10. Guo, X. *et al.* Advances in redox-responsive drug delivery systems of tumor microenvironment. *J. Nanobiotechnology* **16**, 1–10 (2018).
11. Sang, W., Zhang, Z., Dai, Y. & Chen, X. Recent advances in nanomaterial-based synergistic combination cancer immunotherapy. *Chem. Soc. Rev.* **48**, 3771–3810 (2019).
12. Wang, L., Huo, M., Chen, Y. & Shi, J. Tumor Microenvironment-Enabled Nanotherapy. *Adv. Healthc. Mater.* **7**, 1–23 (2018).
13. Jafri, S. H. & Mills, G. Neoadjuvant chemotherapy in lung cancer. *Therapy* **8**, 23–31 (2011).
14. Chlebowski, R. T. & Anderson, G. L. Changing concepts: Menopausal

- hormone therapy and breast cancer. *J. Natl. Cancer Inst.* **104**, 517–527 (2012).
15. Hamanishi, J., Mandai, M. & Konishi, I. Immune checkpoint inhibition in ovarian cancer. *Int. Immunol.* **28**, 339–348 (2016).
 16. Wang, Y.-J. J., Fletcher, R., Yu, J. & Zhang, L. Immunogenic effects of chemotherapy-induced tumor cell death. *Genes Dis.* **5**, 194–203 (2018).
 17. Ezrahi, S., Aserin, A. & Garti, N. Basic principles of drug delivery systems – the case of paclitaxel. *Adv. Colloid Interface Sci.* **263**, 95–130 (2019).
 18. Gong, C. *et al.* Improving anti-tumor activity with polymeric micelles entrapping paclitaxel in pulmonary carcinoma. *Nanoscale* **4**, 6004–6017 (2012).
 19. Richheimer, S. L., Tinnermeier, D. M. & Timmons, D. W. *High-Performance Liquid Chromatographic Assay of Taxol.* vol. 64 <https://pubs.acs.org/sharingguidelines> (1992).
 20. Gornstein, E. & Schwarz, T. L. The paradox of paclitaxel neurotoxicity: Mechanisms and unanswered questions. *Neuropharmacology* **76**, 175–183 (2014).
 21. Sun, B. *et al.* Disulfide Bond-Driven Oxidation- and Reduction-Responsive Prodrug Nanoassemblies for Cancer Therapy. *Nano Lett.* **18**, 3643–3650 (2018).
 22. Fang, W.-S. & Liang, X.-T. *Recent Progress in Structure Activity Relationship and Mechanistic Studies of Taxol Analogues.* vol. 5 1–12 (Bentham Science Publishers Ltd., 2005).
 23. Wang, J. *et al.* Comparison of Redox Responsiveness and Antitumor Capability of Paclitaxel Dimeric Nanoparticles with Different Linkers. *Chem. Mater.* **32**, 10719–10727 (2020).
 24. Wang, Q., Guan, J., Wan, J. & Li, Z. Disulfide based prodrugs for cancer therapy. *RSC Adv.* **10**, 24397–24409 (2020).
 25. Zhang, D. *et al.* Special Section on Pharmacokinetic and Drug Metabolism Properties of Novel Therapeutic Modalities — Minireview Drug Concentration Asymmetry in Tissues and Plasma for Small Molecule – Related Therapeutic Modalities s. *Drug Metab Dispos* **47**, 1122–1135 (2019).
 26. Dougherty, T. J., Grindey, G. B., Fiel, R., Weishaupt, K. R. & Boyle, D. G. Photoradiation Therapy. II. Cure of Animal Tumors With Hematoporphyrin

- and Light23. *JNCI J. Natl. Cancer Inst.* **55**, 115–121 (1975).
27. Plaetzer, K., Krammer, B., Berlanda, J., Berr, F. & Kiesslich, T. Photophysics and photochemistry of photodynamic therapy: fundamental aspects. *Lasers Med. Sci.* **24**, 259–268 (2009).
 28. Agrawal, T. *et al.* Harnessing the Power of Light to Treat Staphylococcal Infections Focusing on MRSA. *Curr. Pharm. Des.* **21**, 2109–2121 (2015).
 29. Wilk, K. A. *et al.* Photo-oxidative action in MCF-7 cancer cells induced by hydrophobic cyanines loaded in biodegradable microemulsion-templated nanocapsules. *Int. J. Oncol.* **41**, 105–116 (2012).
 30. Tian, H. *et al.* Low side-effect and heat-shock protein-inhibited chemophototherapy nanoplatform via co-assembling strategy of biotin-tailored IR780 and quercetin. *Chem. Eng. J.* **382**, (2020).
 31. Jiang, C. *et al.* Hydrophobic IR780 encapsulated in biodegradable human serum albumin nanoparticles for photothermal and photodynamic therapy. *Acta Biomater.* **14**, 61–69 (2015).
 32. Alves, C. G., Lima-Sousa, R., de Melo-Diogo, D., Louro, R. O. & Correia, I. J. IR780 based nanomaterials for cancer imaging and photothermal, photodynamic and combinatorial therapies. *Int. J. Pharm.* **542**, 164–175 (2018).
 33. Li, Y. *et al.* IR-780 Dye as a Sonosensitizer for Sonodynamic Therapy of Breast Tumor. *Sci. Rep.* **6**, 25968 (2016).
 34. Davis, M. E., Chen, Z. & Shin, D. M. Nanoparticle therapeutics: An emerging treatment modality for cancer. *Nat. Rev. Drug Discov.* **7**, 771–782 (2008).
 35. Martella, E. *et al.* Functionalized keratin as nanotechnology-based drug delivery system for the pharmacological treatment of osteosarcoma. *Int. J. Mol. Sci.* **19**, 3670 (2018).
 36. Hoogenboezem, E. N. & Duvall, C. L. Harnessing albumin as a carrier for cancer therapies. *Adv. Drug Deliv. Rev.* **130**, 73–89 (2018).
 37. Larsen, M. T., Kuhlmann, M., Hvam, M. L. & Howard, K. A. Albumin-based drug delivery: harnessing nature to cure disease. *Mol. Cell. Ther.* **4**, 3 (2016).
 38. Elsadek, B. & Kratz, F. Impact of albumin on drug delivery - New applications on the horizon. *J. Control. Release* **157**, 4–28 (2012).
 39. Yu, X. *et al.* An in vitro and in vivo study of gemcitabine-loaded albumin nanoparticles in a pancreatic cancer cell line. *Int. J. Nanomedicine* **10**, 6825–6834 (2015).

40. Kratz, F. *et al.* Probing the cysteine-34 position of endogenous serum albumin with thiol-binding doxorubicin derivatives. Improved efficacy of an acid-sensitive doxorubicin derivative with specific albumin-binding properties compared to that of the parent compound. *J. Med. Chem.* **45**, 5523–5533 (2002).
41. Liu, Z. & Chen, X. Simple bioconjugate chemistry serves great clinical advances: Albumin as a versatile platform for diagnosis and precision therapy. *Chem. Soc. Rev.* **45**, 1432–1456 (2016).
42. Jacobson, O., Kiesewetter, D. O. & Chen, X. Albumin-Binding Evans Blue Derivatives for Diagnostic Imaging and Production of Long-Acting Therapeutics. *Bioconjug. Chem.* **27**, 2239–2247 (2016).
43. Chen, H. *et al.* Chemical conjugation of evans blue derivative: A strategy to develop long-acting therapeutics through albumin binding. *Theranostics* **6**, 243–253 (2016).
44. Zhang, F. *et al.* Transformative Nanomedicine of an Amphiphilic Camptothecin Prodrug for Long Circulation and High Tumor Uptake in Cancer Therapy. *ACS Nano* **11**, 8838–8848 (2017).
45. Moret, F. *et al.* Pheophorbide a and paclitaxel bioresponsive nanoparticles as double-punch platform for cancer therapy. *Pharmaceutics* **13**, (2021).
46. Pei, Q. *et al.* Albumin-bound paclitaxel dimeric prodrug nanoparticles with tumor redox heterogeneity-triggered drug release for synergistic photothermal/chemotherapy. *Nano Res.* **12**, 877–887 (2019).
47. Pei, Q. *et al.* Light-Activatable Red Blood Cell Membrane-Camouflaged Dimeric Prodrug Nanoparticles for Synergistic Photodynamic/Chemotherapy. *ACS Nano* **12**, 1630–1641 (2018).
48. Pei, Q., Hu, X., Zhou, J., Liu, S. & Xie, Z. Glutathione-responsive paclitaxel dimer nanovesicles with high drug content. *Biomater. Sci.* **5**, 1517–1521 (2017).
49. Pei, Q. *et al.* Paclitaxel dimers assembling nanomedicines for treatment of cervix carcinoma. *J. Control. Release* **254**, 23–33 (2017).
50. Wang, H., Xu, M., Xiong, M. & Cheng, J. Reduction-responsive dithiomaleimide-based nanomedicine with high drug loading and FRET-indicated drug release. *Chem. Commun.* **51**, 4807–4810 (2015).
51. Castañeda, L. *et al.* A mild synthesis of N-functionalised bromomaleimides, thiomaleimides and bromopyridazinediones. *Tetrahedron Lett.* **54**, 3493–

- 3495 (2013).
52. Chu, B. *et al.* ROS-Responsive Camptothecin Prodrug Nanoparticles for On-Demand Drug Release and Combination of Chemotherapy and Photodynamic Therapy. *Adv. Funct. Mater.* **30**, 1–13 (2020).
 53. Tarhini, M. *et al.* Protein-based nanoparticle preparation via nanoprecipitation method. *Materials (Basel)*. **11**, 1–18 (2018).
 54. Wang, W., Huang, Y., Zhao, S., Shao, T. & Cheng, Y. Human serum albumin (HSA) nanoparticles stabilized with intermolecular disulfide bonds. *Chem. Commun.* **49**, 2234–2236 (2013).
 55. Aluigi, A. *et al.* Chlorin e6 keratin nanoparticles for photodynamic anticancer therapy. *RSC Adv.* **6**, 33910–33918 (2016).
 56. Miele, E. E. E., Spinelli, G. P., Miele, E. E. E., Tomao, F. & Tomao, S. Albumin-bound formulation of paclitaxel (Abraxane® ABI-007) in the treatment of breast cancer. *Int. J. Nanomedicine* **4**, 99–105 (2009).